



# LUND UNIVERSITY

## Physical bounds of antennas

Gustafsson, Mats; Tayli, Doruk; Cismasu, Marius

2015

[Link to publication](#)

### *Citation for published version (APA):*

Gustafsson, M., Tayli, D., & Cismasu, M. (2015). *Physical bounds of antennas*. (Technical Report LUTEDX/(TEAT-7240)/1-38/(2015); Vol. TEAT-7240). Electromagnetic Theory Department of Electrical and Information Technology Lund University Sweden.

*Total number of authors:*

3

### **General rights**

Unless other specific re-use rights are stated the following general rights apply:

Copyright and moral rights for the publications made accessible in the public portal are retained by the authors and/or other copyright owners and it is a condition of accessing publications that users recognise and abide by the legal requirements associated with these rights.

- Users may download and print one copy of any publication from the public portal for the purpose of private study or research.
- You may not further distribute the material or use it for any profit-making activity or commercial gain
- You may freely distribute the URL identifying the publication in the public portal

Read more about Creative commons licenses: <https://creativecommons.org/licenses/>

### **Take down policy**

If you believe that this document breaches copyright please contact us providing details, and we will remove access to the work immediately and investigate your claim.

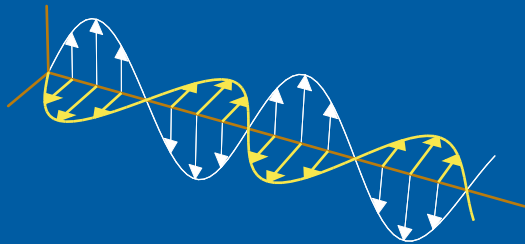
LUND UNIVERSITY

PO Box 117  
221 00 Lund  
+46 46-222 00 00

# Physical bounds of antennas

Mats Gustafsson, Doruk Tayli, and Marius Cismasu

Electromagnetic Theory  
Department of Electrical and Information Technology  
Lund University  
Sweden



Mats Gustafsson  
Mats.Gustafsson@eit.lth.se

Department of Electrical and Information Technology  
Electromagnetic Theory  
Lund University  
P.O. Box 118  
SE-221 00 Lund  
Sweden

Doruk Tayli  
Doruk.Tayli@eit.lth.se

Department of Electrical and Information Technology  
Electromagnetic Theory  
Lund University  
P.O. Box 118  
SE-221 00 Lund  
Sweden

Marius Cismasu  
Marius.Cismasu@eit.lth.se

Department of Electrical and Information Technology  
Electromagnetic Theory  
Lund University  
P.O. Box 118  
SE-221 00 Lund  
Sweden

This is an author produced preprint version of the paper:

M. Gustafsson, D. Tayli, and M. Cismasu. “Physical bounds of antennas”. In: *Handbook of Antenna Technologies*. Ed. by Z. N. Chen. Springer-Verlag, 2015, pp. 1–32

from [http://dx.doi.org/10.1007/978-981-4560-75-7\\_18-1](http://dx.doi.org/10.1007/978-981-4560-75-7_18-1)

This paper has been peer-reviewed but does not include the final publisher proof-corrections or journal pagination.  
Homepage <http://www.eit.lth.se/teat>

Editor: Mats Gustafsson

© Mats Gustafsson, Doruk Tayli, and Marius Cismasu, Lund, December 10, 2015

## Abstract

Design of small antennas is challenging because fundamental physics limits the performance. Physical bounds provide basic restrictions on the antenna performance solely expressed in the available antenna design space. These limits offer antenna designers a-priori information about the feasibility of antenna designs and a figure of merit for different designs. Here, an overview of physical bounds on antennas and the development from circumscribing spheres to arbitrary shaped regions and embedded antennas are presented. The underlying assumptions for the methods based on circuit models, mode expansions, forward scattering, and current optimization are illustrated and their pros and cons are discussed. The physical bounds are compared with numerical data for several antennas.

## 1 Introduction

Physical bounds provide information about the maximum achievable performance of antennas [56, 57, 59, 101, 115]. Bounds are derived, in general, independently of antenna geometry, material, and type. This makes the physical bounds a powerful tool for developing and analyzing all types of antennas. The bounds are expressed in parameters that describe the geometry and electromagnetic properties of the antennas. Moreover, the bounds themselves and their underlying theory provide insight to antenna design and antenna theory. The bounds offer a-priori information of the feasibility of a specific antenna, they give a measure for the figure of merit of an antenna, and they can be used as stopping criteria in heuristic optimization algorithms and for optimization of the antenna position in wireless terminals.

Antenna performance deteriorates with decreasing electrical size, *i.e.*, physical size measured in wavelengths [10, 100]. The bounds are for this reason particularly important for the design of electrically small antennas. There are several definitions of the electrical size of antennas. The classical definition is the radius, measured in wavelengths, of the smallest sphere circumscribing the antenna [56, 57, 59, 101, 115], see also Fig. 1. This is most suitable for antennas with a spherical shape [7]. A generalized measure of electrical size is used for antennas of arbitrary shape and antennas embedded in devices, *e.g.*, mobile phones, tablets, and laptops, see Fig. 1. It should be pointed out that for antennas embedded in devices, the devices may be electrically large whereas the antennas are electrically small.

In small antenna theory, matching bandwidth and the efficiency are two performance parameters often considered for analysis, *e.g.*, [14, 18, 24, 25, 27, 29, 48, 60, 61, 77, 85, 88, 91, 105, 110, 116, 119]. The radiation pattern and the polarization are also of importance in some studies [40, 43, 44]. The bandwidth of an antenna depends on the threshold level of the reflection coefficient (or equivalently the standing wave ratio) [59, 90, 115], and is customarily expressed in terms of the corresponding Q-factor (or antenna Q). This latter parameter is defined as the ratio of the energy stored in the fields created by an antenna, to the energy dissipated by radiation and ohmic heating [90, 115]. The Q-factor is inversely proportional to the fractional bandwidth [48, 119].

The concept of physical bounds for electrically small antennas was introduced by Wheeler [116] and Chu [14] at the end of the 1940s. Wheeler used two-lumped-element circuit models to estimate antenna bandwidth and practical efficiency of small antennas. The classical results by Chu [14] express the lower bound on the Q-factor of antennas in terms of the antenna radius and wavenumber, see Fig. 1. Although these results are useful and provide a first step in analyzing small antennas, they underestimate the lower bound on the Q-factor of non-spherical antennas. More recently, the forward scattering sum rule presented in [35, 43, 44] expresses antenna performance and bounds in terms of the polarizability of the antenna structure or any circumscribing shape, see Fig. 1. These bounds are more realistic than those derived for spherical geometries and are beneficial for analyzing many small antennas that utilize the circumscribing geometry efficiently. On the other hand the forward-scattering sum-rule bounds are less useful for antennas that are embedded in or placed in the proximity of larger structures. Instead, these situations can be studied using antenna current optimization [40]. In this technique the structure is decomposed, into an antenna region with controllable currents and a surrounding structure with induced currents.

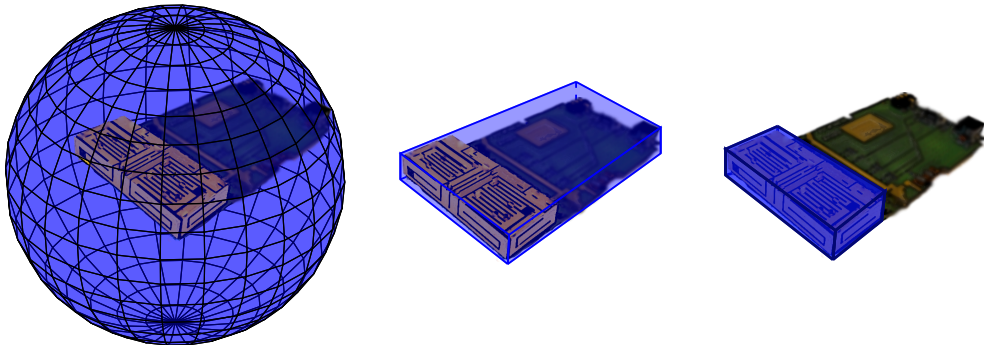


Figure 1: Illustration of circumscribing geometries used for physical bounds. (left) circumscribing sphere introduced by Wheeler [116] and Chu [14] and used for spherical mode expansions. (middle) box circumscribing the antenna structure used in the forward scattering approach [35, 43, 44]. (right) box circumscribing the antenna region used in antenna current optimization [40].

The remainder of this paper is organized as follows. Sec. 2 presents an overview of physical bounds. Sec. 3 reviews the antenna quantities used in the physical bounds. Physical bounds for small antennas based on circuit models and mode expansions are discussed in Sec. 4, forward scattering in 5, and current optimization in 6. Bandwidth bounds for array antennas are discussed in 7. The paper is concluded in Sec. 8. Appendices containing table of notation, radial functions, high-contrast polarizability dyadics, method of moments approximation, and, numerical data for the presented antennas are in App. A, App. B, App. C, App. D, and App. E, respectively.

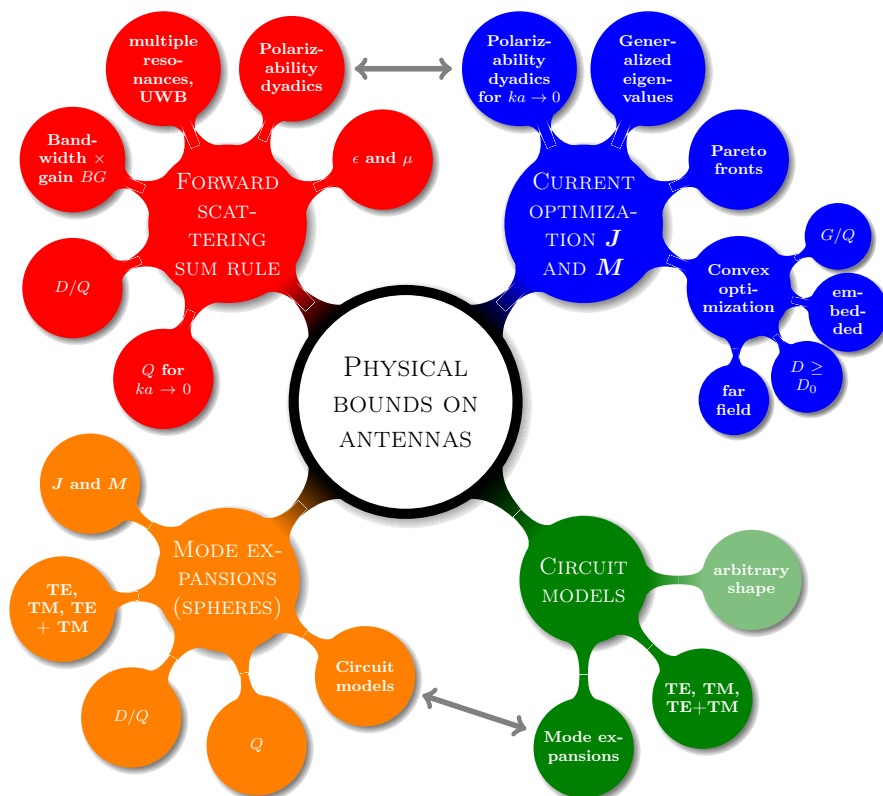


Figure 2: Physical bounds on antennas answer the *Fundamental question: how good can an antenna be?* Bounds can be determined using circuit models (1947), mode expansions (1948), sum rules (2007), and antenna current optimization (2012). Antenna current optimization is the most flexible method (yet) to obtain physical bounds appropriate for many practical antenna design situations.

## 2 Background and overview

Physical bounds on antennas have been analyzed in different ways since the work of Wheeler [116] and Chu [14]. An attempt to categorize the physical bound approaches and methods is made in Fig. 2, even though not all can be described and characterized. Four main techniques have been classified to derive the physical bounds. These are; circuit models, mode expansions, forward scattering, and antenna current optimization.

Circuit models consisting of an inductor or capacitor and a radiation resistance were used by Wheeler [116] to approximate the input impedance of antennas. Based on these circuits he estimated the radiation power factor (related to the inverse of the Q-factor) and bandwidth of antennas. The results obtained by Wheeler, even though approximate, provide physical insight into the dependence of performance on the shape and material loading of antennas. Chu [14] used circuit models of spherical modes to compute the stored energy and Q-factor for spherical geometries. The results obtained from circuit models have been generalized to mixed modes and

non-magnetic sources by Thal [109, 110].

Physical bounds on antennas can be obtained by expanding the fields in spherical modes, also referred to as spherical vector waves, outside a circumscribing sphere of the antenna structure. Chu [14] used this mode expansion together with circuit models to compute the minimum stored energy and to derive the  $Q$  and  $D/Q$  bounds for single spherical modes, where  $D$  is the directivity. He showed that the dipole modes have the lowest  $Q$ -factor and that the  $Q$ -factor of antennas can be reduced by letting the antenna excite a combination of electric (transverse magnetic TM) and magnetic (transverse electric TE) modes. Mode expansions have dominated the research on physical bounds since Chu's work, see *e.g.*, [18, 19, 24, 25, 27, 29, 48, 60, 61, 77, 83, 85, 88, 91, 105, 110, 119] and the historical expose in [115]. The mode expansion approach to physical limitations provides simple analytic formulas for the lower bound on the  $Q$ -factor for single modes [18, 85]. In addition, this approach provides insight into the physics of combinations of different modes (*e.g.*, TE+TM). Thal extended the mode expansions by restricting the electromagnetic fields to originate from electric current densities [110].

Physical bounds were generalized to arbitrary shapes using the forward scattering sum rule in [35, 43, 44]. In this approach, antennas are analyzed in receive mode. It was shown that the interaction over all frequencies between an incident electromagnetic plane wave and an antenna is related to the polarizability of the radiating structure. The bounds derived with this approach are valid for arbitrarily shaped antennas made of reciprocal, linear, and time-translational materials. These bounds are formulated in terms of the directivity– $Q$ -factor quotient,  $D/Q$ , and of the realized gain–bandwidth product. The forward-scattering sum-rule bounds have been verified for several antennas with electrical sizes up to  $ka \approx 1.5$ , where  $k$  is the wavenumber and  $a$  is the radius of the smallest sphere circumscribing the antenna. Yaghjian and Stuart derived similar bounds on the  $Q$ -factor in the limit of small antennas  $ka \ll 1$  using a different technique [118]. These latter bounds were generalized to electric and magnetic currents in [117], see also [73].

Antenna current optimization can be used to derive physical bounds on antennas from optimal current distributions on the radiating structure [40, 47]. This approach is widely applicable to practical antenna design situations and has the potential to include many different requirements on, *e.g.*, performance, size, etc. One of the challenges of this method is to express the antenna quantities involved in defining the parameters of interest, in terms of the current density on the antenna. For example, here the energy expressions introduced by Vandenbosch in [113] for current densities in free space, see also [26, 38, 51, 64], are used to express the  $Q$ -factor of antennas. These energy expressions are further used in minimization of the stored energy to determine current densities optimum in the sense of maximum gain  $Q$ -factor ratio for a fixed radiated field. This and other antenna situations result in convex optimization problems [40] for the current-density, which are easily solvable by common numerical methods [30].

There are alternative approaches to analyze electrically small or large antennas. A few of these approaches are briefly discussed in the following. Reference [112] proposes an approach to physical limitations based on the concepts of superdirectivity



and visible and invisible spatial regions of the fields created by an antenna [107]. A method based on the capacity of the free space communication channel is described in [39, 86]. Considerations about directivity limitations of antennas are presented in [78]. Bandwidth limitations for infinite array antennas are analyzed in [21, 22, 75] using the results in [49, 94], see Sec. 7.

### 3 Antenna quantities for physical bounds

#### 3.1 Antenna parameters

Antenna parameters commonly used in the study of small antennas include the bandwidth, Q-factor, input impedance, reflection coefficient, etc. The parameters used in this section are introduced in the following.

The *reflection coefficient*,  $\Gamma$ , of an antenna is determined from its input impedance,  $Z_a = R_a + jX_a$ , as

$$\Gamma = \frac{Z_a - Z_0}{Z_a + Z_0} = \frac{R_a - Z_0 + jX_a}{R_a + Z_0 + jX_a}, \quad (3.1)$$

where  $Z_0$  is a normalization impedance, usually the characteristic impedance of the transmission line that feeds the antenna. The mismatch depends on the difference between the real part and the commonly real-valued normalization impedance,  $R_a - Z_0$ , and the reactance,  $X_a$ .

The *bandwidth* of an antenna is defined as “*the range of frequencies within which the performance of the antenna, with respect to some characteristic, conforms to a specified standard*” by the IEEE in [67]. Usual performance metrics are matching, efficiency, radiation pattern, polarization, etc. In this chapter, the focus is on the matching bandwidth defined as the frequency interval  $[f_1, f_2]$  for which the amplitude of the reflection coefficient  $|\Gamma|$  is smaller than a given threshold  $\Gamma_0$ , see Fig. 3. The bandwidth of narrow-band antennas is usually expressed as fractional bandwidth,  $B$ , defined as the bandwidth normalized with the center frequency,  $f_0 = (f_1 + f_2)/2$  *i.e.*,

$$B = \frac{f_2 - f_1}{f_0} = \frac{\omega_2 - \omega_1}{\omega_0}, \quad (3.2)$$

where the angular frequency is  $\omega = 2\pi f$ .

The *Q-factor* for an antenna is defined as the ratio between the maximum of the stored electric,  $W_e$ , and magnetic,  $W_m$ , energies and the dissipated power  $P_r + P_\Omega$  [119], *i.e.*,

$$Q = \max\{Q_e, Q_m\} = \frac{2\omega \max\{W_e, W_m\}}{P_r + P_\Omega} = \eta \frac{2\omega \max\{W_e, W_m\}}{P_r}, \quad (3.3)$$

where the electric and magnetic Q-factors are  $Q_e = 2\omega W_e/(P_r + P_\Omega)$  and  $Q_m = 2\omega W_m/(P_r + P_\Omega)$ , respectively, and the efficiency  $\eta = P_r/(P_r + P_\Omega)$ , where  $P_r$  denotes the radiated power and  $P_\Omega$  the ohmic and dielectric power losses. The electric and magnetic Q-factors correspond to the stored energy in the capacitors and inductors, respectively, normalized with the dissipated power in the resistors for lumped circuit networks.



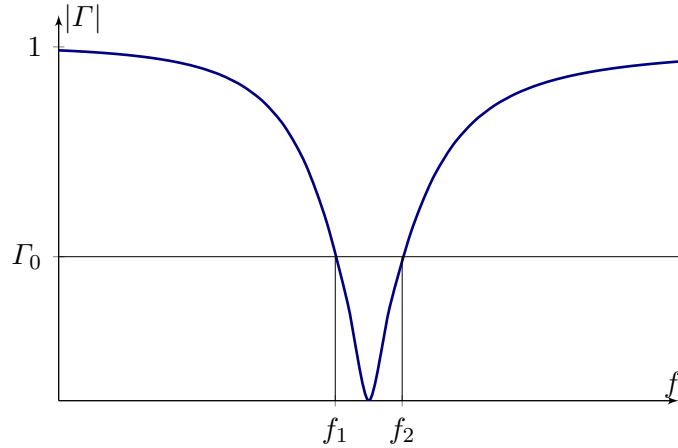


Figure 3: Notations used in the definition of bandwidth and fractional bandwidth (3.2), where  $\Gamma_0$  is the threshold level for the reflection coefficient  $\Gamma$ .

### 3.2 Antenna tuning and matching

Tuning is used to eliminate the reactance mismatch in (3.1). An antenna with input impedance  $Z_a = R_a + jX_a$  is capacitive if  $X_a < 0$  and inductive if  $X_a > 0$ . The simplest way to tune an antenna which is not self-resonant is by connecting a lumped element as in one of the situations depicted in Fig. 4. The tuning capacitance and inductance are chosen such that the tuned input impedance,  $Z_a$ , is purely resistive at the resonance frequency.

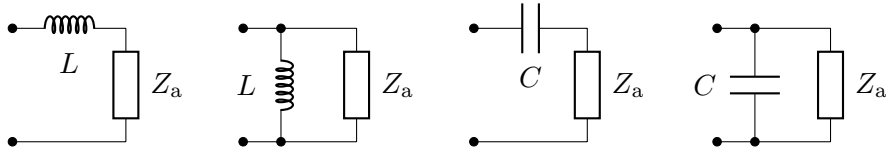


Figure 4: Tuning of an antenna input impedance  $Z_a$  with series or parallel lumped capacitors or inductors.

More complex matching networks can be used to increase the bandwidth of antennas, as illustrated in Fig. 5. The bandwidth potential is a concept that gives information about the bandwidth achievable with a two-lumped-element matching network [93]. The upper bound on the fractional bandwidth for lossless matching networks is given by the Bode-Fano limit [23, 48, 56]

$$B \leq \frac{27}{Q|\Gamma_{0,\text{dB}}|}, \quad (3.4)$$

for an RLC antenna input impedance with the threshold level  $\Gamma_{0,\text{dB}} = 20 \log_{10} \Gamma_0$ .

The bandwidth is inversely proportional to the Q-factor, *i.e.*, a high Q-factor implies a narrow bandwidth. The precise proportionality is determined by the shape

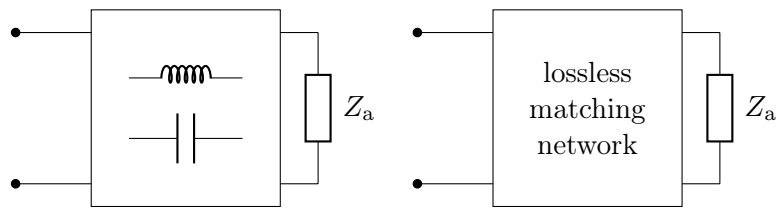


Figure 5: Left—matching networks containing two lumped elements used for estimating the bandwidth potential [93]. Right—black-box-type matching network, *i.e.*, with arbitrary complexity and topology, that may reach some design requirements, *e.g.*, reach close to the Bode-Fano limit [23, 48, 56].

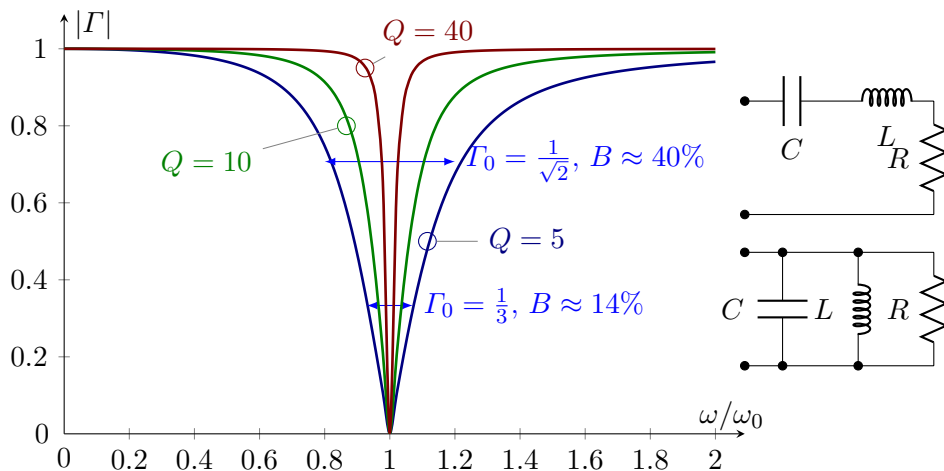


Figure 6: Reflection coefficient,  $|\Gamma|$ , for RLC circuits (inset right) with  $Q = \{5, 10, 40\}$ . The corresponding fractional bandwidths for  $\Gamma_0 = \{1/\sqrt{2}, 1/3\}$  are depicted.

of the reflection coefficient, *i.e.*, by its dependence on frequency, that is often quantified with the distribution of the resonances. The simplest case of a single resonance corresponds to series or parallel RLC circuits, see right inset of Fig. 6, where the fractional bandwidth for a single resonance is [119]

$$B \approx \frac{2}{Q} \frac{\Gamma_0}{\sqrt{1 - \Gamma_0^2}} = \frac{2}{Q} \quad \text{for } \Gamma_0 = 1/\sqrt{2}. \quad (3.5)$$

The reflection coefficients for single resonance RLC circuits with  $Q = 5, 10$  and  $40$  are depicted in Fig. 6.

The estimate (3.5) is very accurate for  $Q \gg 2$  for the RLC circuit. The special case of the half-power bandwidth  $B \approx 2/Q$  predicts an infinite bandwidth for  $Q = 1$ . This suggests that the Q-factor is most useful for  $Q \gg 1$ . Reasonable accuracy in (3.5) is obtained for  $Q > 5$  or  $Q > 10$ , in practice. The assumption of a single resonance is however essential for (3.5) such that the use of multiple resonances to increase the bandwidth [56] is described less accurately by this expression.

Differentiation of the input impedance offers an alternative method to estimate the Q-factor of antennas [48, 76, 119]:

$$Q_{Z'} = \omega |\Gamma'| = \frac{\omega |Z'_m|}{2R} = \frac{|\omega Z' + j|X||}{2R} = \frac{\sqrt{(\omega R')^2 + (\omega X' + |X|)^2}}{2R}, \quad (3.6)$$

where  $Z_m$  denotes the input impedance tuned to resonance with a series capacitor or inductor, as in Fig. 4, see also [51]. Expression (3.6) is exact for the series RLC-series and often very accurate for antennas with  $Q \gg 1$ . However, this expression can underestimate the Q-factor for multiple resonances [37, 48, 51, 106].

The  $Q_{Z'}$  estimate (3.6) can be interpreted as a local Padé approximation of the reflection coefficient (or input impedance) with a lumped-element circuit [48]. This expression estimates the bandwidth (3.5) for  $B \ll 1$ , or similarly  $\Gamma_0 \ll 1$ . Accurate estimates of the fractional bandwidth (3.5) using  $Q_{Z'}$  require that the first order derivative  $|Z'_m|$  (linear term) dominates over the second and higher order derivatives. This requirement is not always met and there are synthesized cases with  $|Z'_m| \approx 0$  where  $Q_{Z'}$  overestimates the fractional bandwidth using (3.5) [37, 48, 51].

### 3.3 Stored electric and magnetic energies

Physical bounds on antennas are often derived using the electromagnetic fields that surround the antenna [18, 24, 25, 27, 61, 77, 85, 105, 110, 115, 119]. Consider an antenna confined to the region  $\Omega$  as depicted in Fig. 7. The antenna current density is denoted  $\mathbf{J}(\mathbf{r})$  and the radiated electric field is  $\mathbf{E}(\mathbf{r})$  that simplifies to

$$\mathbf{E}(\mathbf{r}) = \frac{e^{-jkr}}{r} \mathbf{F}(\hat{\mathbf{r}}) \quad \text{as } r \rightarrow \infty, \quad (3.7)$$

where  $\mathbf{F}$  is the electric far field,  $r = |\mathbf{r}|$ , and  $\hat{\mathbf{r}} = \mathbf{r}/r$ . The time average electric and magnetic energy densities in free space are  $w_e = \epsilon_0 |\mathbf{E}|^2/4$  and  $w_m = \mu_0 |\mathbf{H}|^2/4$ , respectively, where  $\mathbf{H}(\mathbf{r})$  is the magnetic field. These energy densities resemble the time average energies stored in capacitors and inductors,  $W_e = C|V|^2/4$  and  $W_m = L|I|^2/4$ , respectively. The energy in a region is obtained by integrating the energy density in that region. The  $1/r$  decay of the field (3.7) implies that the total electromagnetic energy for antennas in free space is unbounded and hence dominated by the contributions from the radiated field far away from the antenna.

The stored electromagnetic energy is the part of the energy that is not radiated. This energy is confined to the near-field region around the antenna. The stored energy has been evaluated in the history of antenna technology by different methods. Chu [14] and Thal [110] used circuit models of the spherical modes to determine the stored energy for spherical regions. Synthesized lumped-circuit models give an alternative method to estimate the Q-factor from the input impedance of antennas [37]. Collin and Rothschild [18] calculate the stored energy by subtraction of the energy density of the power flow giving

$$W_e^{(P)} = \frac{\epsilon_0}{4} \int_{\mathbb{R}^3} |\mathbf{E}(\mathbf{r})|^2 - \eta_0 \operatorname{Re}\{\mathbf{E}(\mathbf{r}) \times \mathbf{H}(\mathbf{r})^* \cdot \hat{\mathbf{r}}\} dV, \quad (3.8)$$

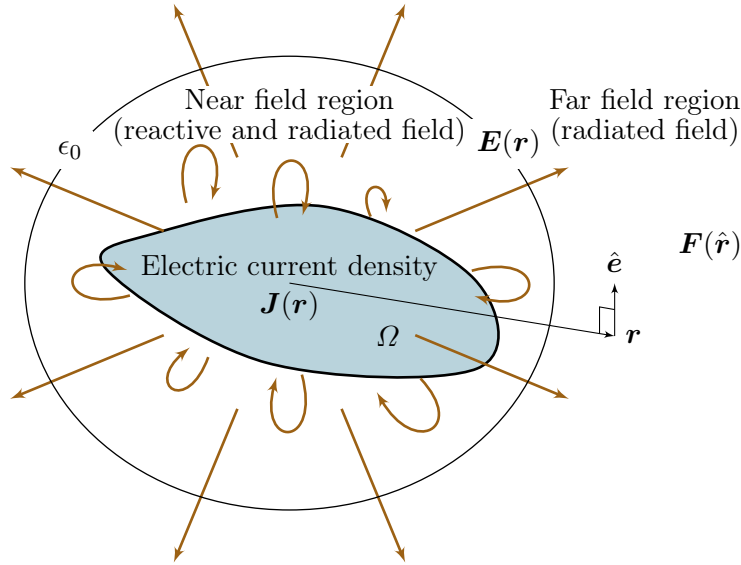


Figure 7: Reactive and radiated fields from a current density  $\mathbf{J}(\mathbf{r})$  in the region  $\Omega$ . Note that, in the far field,  $\hat{\mathbf{e}}$  is perpendicular to  $\mathbf{r}$ .

for the electric stored energy, where the asterisk  $*$  denotes complex conjugation and  $\mathbb{R}_r^3 = \{\mathbf{r} : \lim_{r_0 \rightarrow \infty} |\mathbf{r}| \leq r_0\}$  denotes an infinitely large spherical volume, see also [24, 27, 38, 77, 85, 119]. The magnetic energy is expressed in terms of a magnetic energy density analogous to (3.8). The integral expressions by Vandenbosch [113] represent the stored energy as quadratic forms in terms of current densities. These expressions are particularly useful as radiated fields are generated by current densities on the antenna structure. Furthermore, these integral expressions are directly applicable to antenna current optimization [40, 47]. They are identical to subtraction of the energy density of the radiated field for many cases [38] and reduces to the stored energy in [12, 26] in the limit of small antennas. Here, the stored electric and magnetic energies given by the integral expressions [38, 113]

$$W_e = \frac{\eta_0}{4\omega} \int_{\Omega} \int_{\Omega} \nabla_1 \cdot \mathbf{J}(\mathbf{r}_1) \nabla_2 \cdot \mathbf{J}(\mathbf{r}_2)^* \frac{\cos(k|\mathbf{r}_1 - \mathbf{r}_2|)}{4\pi k|\mathbf{r}_1 - \mathbf{r}_2|} - (k^2 \mathbf{J}(\mathbf{r}_1) \cdot \mathbf{J}(\mathbf{r}_2)^* - \nabla_1 \cdot \mathbf{J}(\mathbf{r}_1) \nabla_2 \cdot \mathbf{J}(\mathbf{r}_2)^*) \frac{\sin(k|\mathbf{r}_1 - \mathbf{r}_2|)}{8\pi} dV_1 dV_2 \quad (3.9)$$

and

$$W_m = \frac{\eta_0}{4\omega} \int_{\Omega} \int_{\Omega} k^2 \mathbf{J}(\mathbf{r}_1) \cdot \mathbf{J}(\mathbf{r}_2)^* \frac{\cos(k|\mathbf{r}_1 - \mathbf{r}_2|)}{4\pi k|\mathbf{r}_1 - \mathbf{r}_2|} - (k^2 \mathbf{J}(\mathbf{r}_1) \cdot \mathbf{J}(\mathbf{r}_2)^* - \nabla_1 \cdot \mathbf{J}(\mathbf{r}_1) \nabla_2 \cdot \mathbf{J}(\mathbf{r}_2)^*) \frac{\sin(k|\mathbf{r}_1 - \mathbf{r}_2|)}{8\pi} dV_1 dV_2, \quad (3.10)$$

respectively, are used, where it is noted that  $\eta_0/\omega = \mu_0/k$ . The corresponding

radiated power is [28, 38, 113]

$$P_r = \frac{\eta_0}{2} \int_{\Omega} \int_{\Omega} (k^2 \mathbf{J}(\mathbf{r}_1) \cdot \mathbf{J}(\mathbf{r}_2)^* - \nabla_1 \cdot \mathbf{J}(\mathbf{r}_1) \nabla_2 \cdot \mathbf{J}(\mathbf{r}_2)^*) \frac{\sin(k|\mathbf{r}_1 - \mathbf{r}_2|)}{4\pi k|\mathbf{r}_1 - \mathbf{r}_2|} dV_1 dV_2. \quad (3.11)$$

These energy expressions resemble the impedance matrices obtained from the electric field integral equation (EFIE) [51, 62, 64]. The stored energies are also generalized to electric and magnetic currents [73, 74] and lossy media [51].

### 3.4 Sum rules

Sum rules have been used to derive physical bounds on electromagnetic systems such as matching [23], radar absorbers and array antennas [22, 75, 94], antennas [33, 43, 44], scattering [34, 103], high-impedance surfaces [49], and metamaterials [41, 52, 104]. The sum rules are integral identities that often relate the parameter of interest integrated over all frequencies with some low-frequency quantity.

The sum rules presented here are based on integral identities for Herglotz functions [5, 87] or similarly positive real functions [120]. Positive real functions [120],  $Z(s)$ , are analytic and  $\operatorname{Re}\{Z(s)\} \geq 0$  for  $\operatorname{Re} s > 0$ . They are often found in linear, passive, and causal systems [5, 120]. The identities

$$\frac{1}{\pi} \int_{\mathbb{R}} \frac{\operatorname{Re} Z(j\omega)}{\omega^2} d\omega \stackrel{\text{def}}{=} \lim_{\varepsilon \rightarrow 0^+} \lim_{y \rightarrow 0^+} \frac{1}{\pi} \int_{\varepsilon < |\omega| < 1/\varepsilon} \frac{\operatorname{Re} Z(j\omega + y)}{\omega^2} d\omega = a_1 - b_1 \leq a_1 \quad (3.12)$$

are valid for all PR functions having the asymptotic expansions

$$Z(s) = a_1 s + o(s) \quad \text{as } s \hat{\rightarrow} 0 \quad \text{and} \quad Z(s) = b_1 s + o(s) \quad \text{as } s \hat{\rightarrow} \infty, \quad (3.13)$$

where  $\hat{\rightarrow}$  means limits in some sector  $|\arg s| < \pi/2 - \alpha$  for  $\alpha > 0$  and the integral (3.12) is interpreted as a limit from the complex valued right half plane, see [5] for details.

## 4 Circuit models and mode expansions

Wheeler used circuit models to analyze small antennas [116]. The electric antenna consists of a lumped capacitance in parallel with a radiation resistance. The corresponding magnetic antenna is a lumped inductance in series with a radiation resistance. These results provide intuition and rules of thumb.

Chu [14] determined the minimum stored energy around an antenna in three steps:

1. circumscribe the antenna by a sphere with radius  $a$ , see Fig. 8.
2. expand the radiated electromagnetic field outside the circumscribing sphere in spherical modes [11, 55, 61, 108], see Fig. 9.
3. compute the stored energy outside the sphere from a lumped circuit representation of the spherical modes [108].

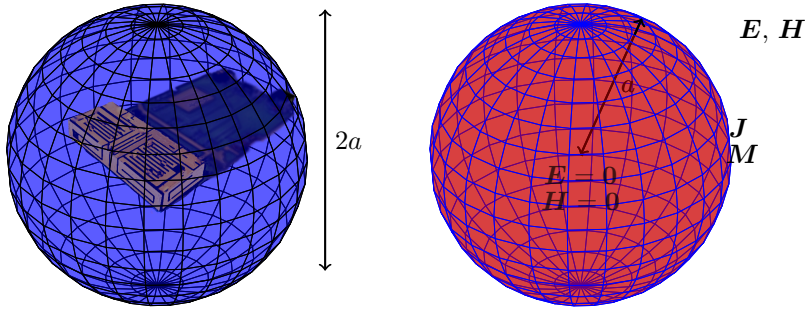


Figure 8: (left) sphere with radius  $a$  that circumscribes the antenna. (right) the Chu model [14] with vanishing field in the interior of the sphere or similarly use of electric  $\mathbf{J}$  and magnetic  $\mathbf{M}$  surface currents.

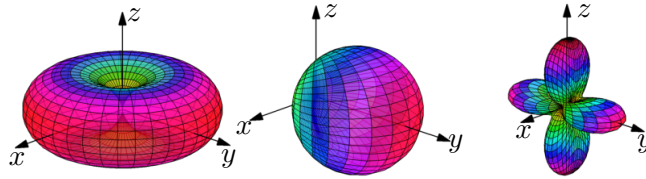


Figure 9: Radiation patterns of spherical modes. (left) electric,  $\text{TM}_{0,1}$ , and magnetic,  $\text{TE}_{0,1}$ , dipole modes. (middle) Huygens source  $\text{TM}_{0,1} + \text{TE}_{1,1}$ . (right) quadrupole mode  $\text{TM}_{1,2}$ .

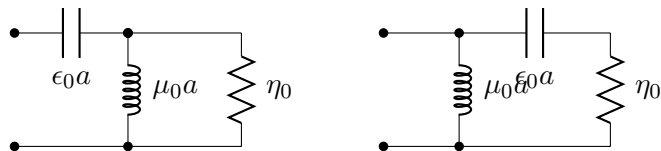


Figure 10: Lumped-element circuit models of the electric ( $\text{TM}_{m,1}$ ) and magnetic dipole ( $\text{TE}_{m,1}$ ) modes [14, 61, 108].

The lumped-element circuit models of the electric (TM<sub>*m*,1</sub>) and magnetic dipole (TE<sub>*m*,1</sub>) modes [14, 85, 108] are depicted in Fig. 10. The electric and magnetic cases having identical *n*-index are dual such that the corresponding Q-factors are identical. The electric dipole has the stored electric and magnetic energies, and radiated power

$$W_e = \frac{\eta_0 |I|^2}{4\omega} \frac{1}{ka}, \quad W_m = \frac{\eta_0 |I|^2}{4\omega} \frac{ka}{1 + k^2 a^2}, \quad \text{and } P_r = \frac{\eta_0 |I|^2}{2} \frac{k^2 a^2}{1 + k^2 a^2}, \quad (4.1)$$

respectively, for a current source *I*. The electric energy dominates over the magnetic energy,  $W_e > W_m$ , *i.e.*, the electric dipole mode is capacitive. The stored energy and radiated power give the Chu-bound for single mode antennas, stating that the Q-factor of a single mode antenna circumscribed by a sphere with radius *a* satisfies

$$Q \geq Q_{\text{Chu}} = \frac{2\omega \max\{W_e, W_m\}}{P_r} = \frac{2\omega W_e}{P_r} = \frac{1}{(ka)^3} + \frac{1}{ka}. \quad (4.2)$$

The inequality  $Q \geq Q_{\text{Chu}}$  is interpreted as the contribution to the Q-factor from the stored energy within the spherical volume. This means that antenna designs reaching the Chu lower bound should have negligible electric field inside the sphere [14].

Circuit models and closed form expressions are convenient for dipole modes. However, these methods become increasingly complicated for higher order modes, see also Fig. 9. The input impedance of the circuits modeling spherical modes offers an approximation of the Q-factor. Chu approximated the *Q* by differentiation of the reactance [14] to show that  $Q_n \sim (ka)^{-2n-1}$  as  $ka \rightarrow 0$  for modes of order *n*, see also [48] for the corresponding results from differentiation of the input impedance (3.6). Chu also discussed the case of mixed TM and TE modes, *e.g.*, the Huygens source in Fig. 9, and showed that mixed modes can lower the bound on *Q* by a factor of two for  $ka \ll 1$  [14, 61] by, *e.g.*, using an inductive TE mode instead of a lumped inductor as the tuning element in Fig. 4. The resulting Q-factor is bounded as

$$Q \geq \frac{1}{2(ka)^3} + \frac{1}{ka} \quad (4.3)$$

for larger  $ka$  [85, 91].

Mode expansions have dominated the research on physical bounds since these expansions were introduced by Chu, see *e.g.*, [18, 24, 25, 27, 48, 61, 77, 85, 88, 91, 105, 110, 119] and the historical expose in [115]. In particular Collin & Rothschild [18] used spherical mode expansions and analytic evaluation of (3.8) to derive closed form expressions of the Q-factor for spherical modes of arbitrary order, *e.g.*,

$$Q_1 = \frac{1}{(ka)^3} + \frac{1}{ka}, \quad Q_2 = \frac{18}{(ka)^5} + \frac{6}{(ka)^3} + \frac{3}{ka}, \quad \text{and } Q_n \sim \frac{1}{(ka)^{2n+1}}, \quad (4.4)$$

where the rapid increase in the Q-factor for small antennas  $ka \ll 1$  and higher order modes  $n > 1$  is noted.

Equivalent (surface) currents [11] offer a powerful interpretation of physical bounds. The Chu bound (4.2) is derived under the assumption of negligible stored



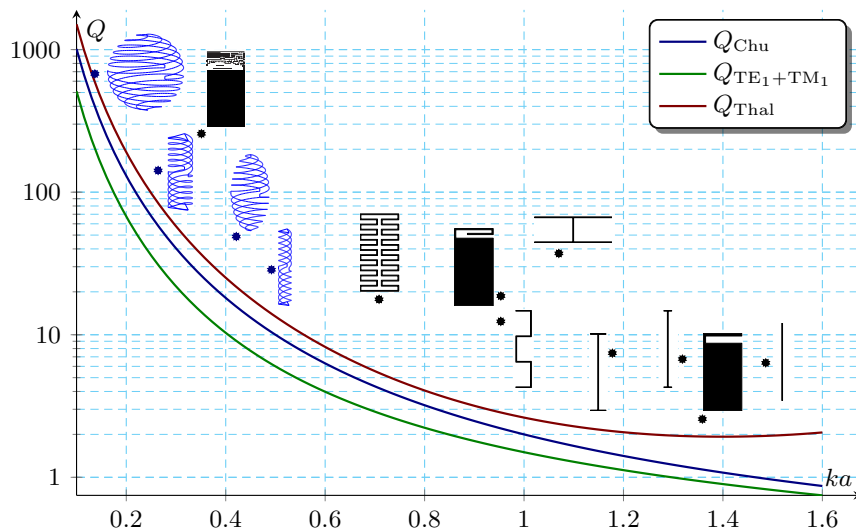


Figure 11: The Chu (4.2), Thal (4.6), and mixed mode bounds on  $Q$  compared with numerical estimates using  $Q_{Z'_{in}}$  (3.6), see Tab. 3 and Tab. 4 [2]. Wire antennas (blue) and planar antennas (black) are depicted. The different types of dipoles (black) are constructed with planar strips.

energy in the interior of a sphere. This requires electric,  $\mathbf{J}$ , and magnetic,  $\mathbf{M}$ , surface currents to exist on this sphere in free space, see Fig. 8. Antennas without magnetic currents (or magnetic material) have internal fields and hence an internal stored energy. Thal [110] extended the Chu bound to the case of only electric surface currents by adding the energy stored in the interior of a sphere. The resulting bound for the electric dipole mode is

$$Q \geq \frac{3}{2(ka)^3} = \frac{3}{2}Q_{\text{Chu}} \quad \text{for } ka \ll 1, \quad (4.5)$$

see also [58, 60]. The closed form expressions for arbitrary spherical modes are [38]

$$Q_{\tau n, e}^{(P)}(\kappa) = \kappa - \frac{(\kappa R_{\tau n}^{(1)}(\kappa) R_{\tau n}^{(2)}(\kappa))'}{2(R_{\tau n}^{(1)}(\kappa))^2} \quad \text{and} \quad Q_{\tau n, m}^{(P)} = Q_{\tau n, e}^{(P)}(\kappa) - \frac{R_{\tau n}^{(2)}(\kappa)}{R_{\tau n}^{(1)}(\kappa)} \quad (4.6)$$

for the electric and magnetic Q-factors, respectively, with  $\kappa = ka$ . Here the expressions for the TE ( $\tau = 1$ ) and TM ( $\tau = 2$ ) modes are written in identical forms by using radial functions [55], see App. B.

The Chu (4.2), Thal (4.5), and mixed mode bounds are compared with several antennas in Fig. 11, see also [97]. All antennas have Q-factors above the bounds, as expected. The folded spherical helix antenna fills the spherical surface and performs close to the Thal bound (4.5). While the dipole and planar antennas do not utilize the spherical volume as efficiently as spherical helices. This results such that the former have Q-factors above the bounds. On the other hand, for the cylindrical structures; cylindrical helix and spheroidal helix, the antenna performance

is between the performance of spherical and planar structures. It should be noted that increasing the thickness of the wire and strip antennas decrease their Q-factors. There are several suggestions for antennas with Q-factors approaching the Chu lower bound or corresponding bounds for TE and mixed mode cases. The folded spherical helix, see Fig. 11, investigated by Best [7] has a Q-factor close to the Thal bound, see also [1]. Kim proposed a few designs reaching close to the physical bounds on  $Q$  [80, 81].

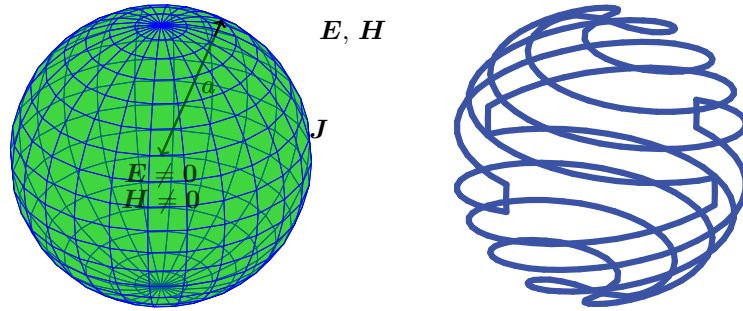


Figure 12: (left) the Thal model [110] with an electromagnetic field in the interior of the sphere and electric  $\mathbf{J}$  surface currents. (right) the folded spherical helix [7] with electric  $\mathbf{J}$  surface currents and Q-factor  $Q \approx 1.5Q_{\text{Chu}}$ .

Most antennas are not spherical and, as seen in Fig. 11, their Q-factors are far from the bound. This has encouraged researchers to extend the mode expansions to non-spherical regions. Collin and Rothschild [18] used cylindrical waves to derive bounds for infinite cylinders and Foltz & McLean [25] and Sten, Koivisto, and Hujanen [105] used expansions in spheroidal coordinates to derive bounds for antennas confined to spheroidal volumes. However, it turns out to be difficult to extend the results from spherical regions using mode expansions. An alternative approach based on sum rules for spherical waves is investigated in [3, 4], where the bandwidth is shown to be related to the polarizability. The case with spherical regions in the vicinity of a ground plane is analyzed in [105]. There are also extensions to antennas embedded in lossy media [77].

## 5 Forward scattering sum rule

The forward scattering bounds in [20, 43, 44] are solely based on the assumptions of linearity, time-translational invariance, causality, and reciprocity. These are generally accepted assumptions in the antenna community and valid for a large class of antennas, *e.g.*, antennas with metallic and dielectric components, antennas fed by a single transmission line and impedance matched with a matching network, etc. Some of the main advantages of these forward scattering bounds are that they: are simple to use; provide physical insight into small antennas given by expressions in terms of polarizability dyadics; hold for arbitrary enclosing geometries; and are formulated in terms of the realized gain (the parameter quantifying the system gain)

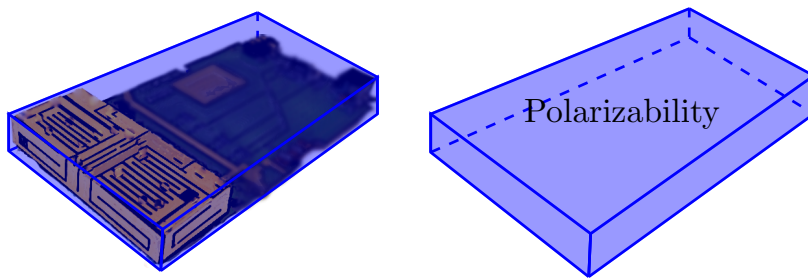


Figure 13: (left) Circumscribing box for an antenna. (right) Polarizability of the circumscribing structure to determine the physical bounds (5.4).

and bandwidth or the directivity and Q-factor.

Physical bounds on arbitrarily shaped antennas were introduced in [44] and further developed in [20, 32, 35, 42, 43, 102]. These results are based on the forward scattering sum rule [34, 103] that states that the all spectrum interaction between objects and electromagnetic fields is proportional to the electro-,  $\gamma_e$ , and magneto-static,  $\gamma_m$ , polarizability dyadics, *i.e.*,

$$\frac{1}{\pi} \int_{\mathbb{R}} \frac{\sigma_a(k) + \sigma_s(k)}{k^2} dk = \hat{\mathbf{e}}^* \cdot \gamma_e \cdot \hat{\mathbf{e}} + (\hat{\mathbf{r}} \times \hat{\mathbf{e}}^*) \cdot \gamma_m \cdot (\hat{\mathbf{r}} \times \hat{\mathbf{e}}) \quad (5.1)$$

for all objects composed of linear, passive, and time translational invariant media [34, 42, 103]. Here,  $\sigma_a$  and  $\sigma_s$  are the absorption and scattering cross sections, respectively. This identity was derived for dielectric spheroids in [92] and generalized to arbitrary objects and polarizations in [34, 42, 103].

An antenna identity is obtained from the forward scattering sum rule by using reciprocity and the relation between the effective aperture (or absorption cross-section) and partial directivity for lossless antennas

$$\sigma_a(k, \hat{\mathbf{r}}, \hat{\mathbf{e}}) = \frac{\pi}{k^2} (1 - |\Gamma(k)|^2) D(k, -\hat{\mathbf{r}}, \hat{\mathbf{e}}). \quad (5.2)$$

Combining (5.1) and (5.2) gives

$$\int_0^\infty \frac{(1 - |\Gamma(k)|^2) D(k, \hat{\mathbf{r}}, \hat{\mathbf{e}})}{k^4} dk = \frac{\eta}{2} (\hat{\mathbf{e}} \cdot \gamma_e \cdot \hat{\mathbf{e}} + (\hat{\mathbf{r}} \times \hat{\mathbf{e}}) \cdot \gamma_m \cdot (\hat{\mathbf{r}} \times \hat{\mathbf{e}})), \quad (5.3)$$

for the linear polarization  $\hat{\mathbf{e}}$ , where, the generalized (or all spectrum) absorption efficiency  $\eta$  [34, 43, 44] is introduced. This is further transformed to a bound on the  $D/Q$  (directivity bandwidth product) expressed in terms of the high contrast polarizability dyadic,  $\gamma_\infty \geq \gamma_e$ , see App. C, by assuming a resonance model [43, 44] and:

$$\frac{D}{Q} \leq \frac{\eta k^3}{2\pi} \hat{\mathbf{e}} \cdot \gamma_\infty \cdot \hat{\mathbf{e}} \leq \frac{\eta k^3}{2\pi} \max \text{eig } \gamma_\infty \quad (5.4)$$

for non-magnetic media,  $\gamma_m = \mathbf{0}$ , see [43, 44] for the case of electric and magnetic media. The lower bound on the Q-factor

$$Q \geq \frac{6\pi}{k^3 \max \text{eig } \gamma_\infty} \quad (5.5)$$

is based the fact that small electric dipoles have directivity  $D = 3/2$  and generalized absorption efficiency  $\eta \leq 1/2$  [35]. Results similar to those introduced in the previous paragraph are derived by Yaghjian and Stuart [118] and using antenna current optimization [47], see also [111, 114, 117]. This bound is identical to that derived by Thal [110] for small spherical structures (4.5) with electric currents radiating as an electric dipole, *i.e.*,

$$Q \geq \frac{3}{2k^3 a^3} = \frac{3}{2} Q_{\text{Chu}} \quad \text{for } ka \ll 1, \quad (5.6)$$

where the high-contrast polarizability dyadic  $\gamma_\infty = 4\pi a^3 \mathbf{I}$  for a sphere with the radius  $a$  is used.

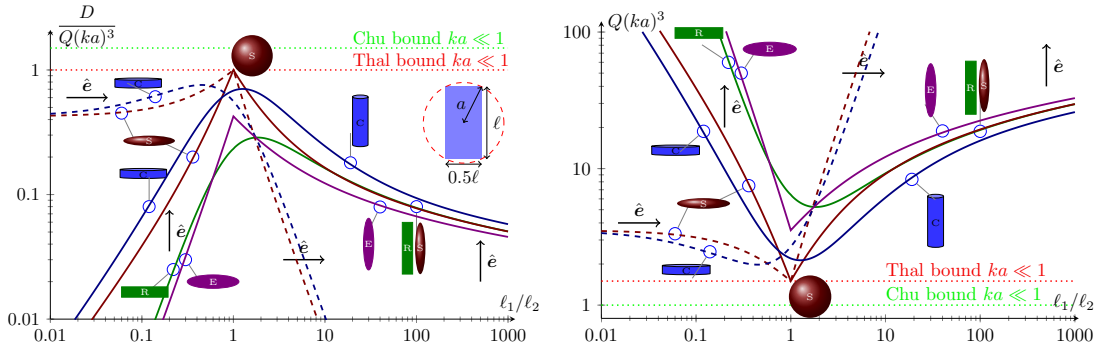


Figure 14: Forward scattering bound on  $D/Q$  (left) and  $Q$  (right) normalized with  $(ka)^3$  for non-magnetic spheroidals, cylinders, planar rectangles, and planar ellipses with height  $l_1$  and width  $l_2$  [32] using  $\eta = 1/2$ . Vertical polarization in solid lines and horizontal polarization in dashed lines.

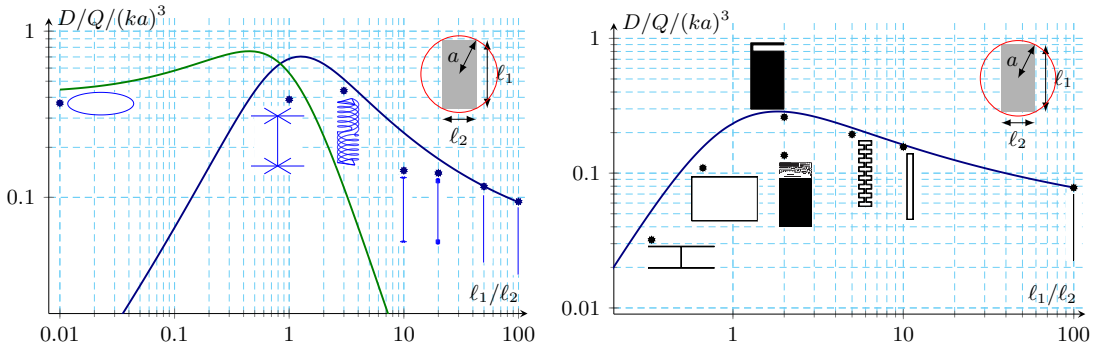


Figure 15: Forward scattering bounds on  $D/Q$  using  $\eta = 1/2$  normalized with  $(ka)^3$  compared with numerical results from FEKO [2] for non-magnetic cylindrical (left), see Tab. 3, and planar (right), see Tab. 4, structures.

The computed bounds (5.4) and (5.5) for spheroidals [44], cylinders [43], planar rectangles [43], and planar ellipses [32] are depicted in Fig. 14, see also Tab. 2. The

Chu (4.2) and Thal (4.5) bounds for  $ka \ll 1$  are also included for comparison. The results illustrate how the bound depends on the shape and polarization of the electric field. The spheroid simplifies to a sphere for  $\ell_1 = \ell_2$  with the bound  $D/(Qk^3a^3) = 1$  that is identical to the result (4.5) and (5.6) by Thal [110] using the directivity  $D = 3/2$ . Several antennas are compared with the bound in Fig. 15, see also [6, 9, 35, 43, 95]. The comparisons show that many antennas perform close to the bounds.

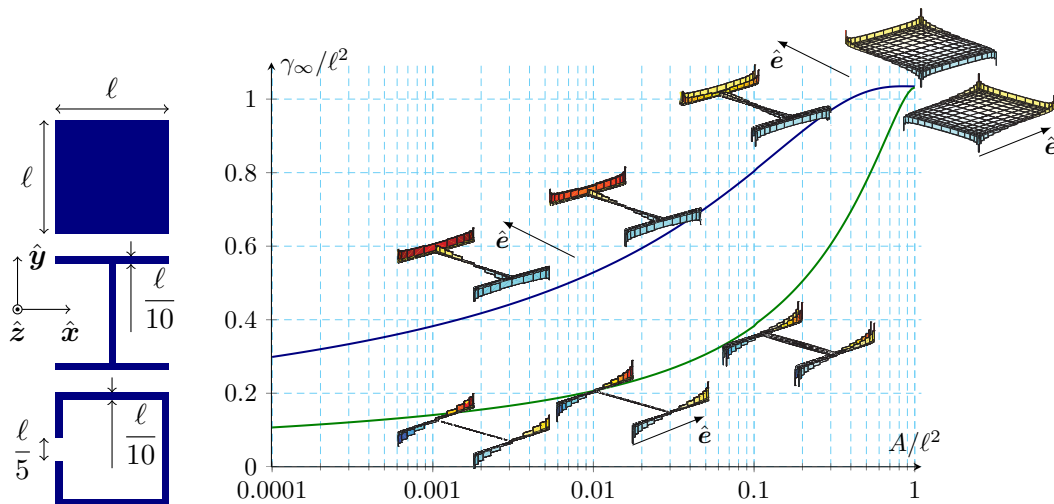


Figure 16: (left) Polarizability dyadics for planar rectangular structures with polarizability dyadics  $\gamma_\infty \approx 1.04\ell^3(\hat{x}\hat{x} + \hat{y}\hat{y})$ ,  $\gamma_\infty \approx \ell^3(0.51\hat{x}\hat{x} + 0.93\hat{y}\hat{y})$ , and  $\gamma_\infty \approx \ell^3(0.94\hat{x}\hat{x} + 0.96\hat{y}\hat{y})$ , for the rectangle, capped dipole, and loop, respectively. (right) Polarizability for planar capped dipoles with area  $A$  circumscribed by a rectangle with sides  $\ell \times \ell$ . Resulting charge distributions are also depicted in the figure, see [53].

The forward scattering identity (5.1) and bound (5.4) show that the antenna performance is proportional to the polarizability of the antenna structure. Polarizability quantifies the charge-separation properties of a structure, *i.e.*, the induced dipole moment is proportional to the polarizability,  $\mathbf{p} = \epsilon_0\gamma_e \cdot \mathbf{E}$ . For example, large metallic regions at the extremities of an antenna increase the maximum achievable  $D/Q$ -performance of that antenna, for linear polarization in the direction of the antenna extremities. This is illustrated for a planar capped dipole structure in Fig. 16, see also [53]. The polarizability for a planar square metallic rectangle in the  $xy$ -plane with side lengths  $\ell$  is  $\gamma_\infty \approx 1.04\ell^3(\hat{x}\hat{x} + \hat{y}\hat{y})$ . The polarizability for the capped dipole,  $\gamma_\infty \approx \ell^3(0.51\hat{x}\hat{x} + 0.93\hat{y}\hat{y})$ , is lower as some metal is removed. The polarizability is higher in the  $\hat{y}$ -direction than in the  $\hat{x}$ -direction as the metal strips at the edges allow a large charge separation in the  $\hat{y}$ -direction. This is further illustrated in the right part of Fig. 16, where the polarizability for planar capped dipoles with area  $A$  are depicted. Note that the capped dipoles have zero volume and that the polarizability reduces with approximately a factor of 3 whereas the area decreases a factor of  $10^4$ . The antenna performance for an electric dipole antenna

is hence not simply related to the volume or area but to the structures ability to separate charge.

Closed-form expressions are available for the polarizability dyadics of structures such as spheroids, planar ellipses, half spheres, etc., [72, 82, 98, 103]. An illustrative example is given by the polarizability of a dielectric sphere with radius  $a$  [11, 13, 31, 68], *i.e.*,

$$\boldsymbol{\gamma}_e = 4\pi a^3 \frac{\epsilon_r - 1}{\epsilon_r + 2} \mathbf{I} \leq 4\pi a^3 \mathbf{I} = \boldsymbol{\gamma}_\infty. \quad (5.7)$$

This simple example illustrates two important properties of the polarizability dyadic with implication for antenna design, *i.e.*, the polarizability is increasing in the permittivity  $\epsilon_r$  and the size  $a$  [71, 99]. For other structures the polarizability is calculated numerically using the method of moments [32, 63, 66, 96] or the finite element method [103], see App. C. The polarizability and the associated bound on  $D/Q$  are approximated by rational functions for cylinders and planar rectangles in [32], see also the MATLAB code [45].

The forward scattering bounds are generalized to electric and magnetic media by inclusion of the magnetic polarizability  $\boldsymbol{\gamma}_m$  in (5.4) and (5.5), see [43, 44]. The generalization to elliptic polarization is discussed in [42]. Ultra-wideband and multi-band antennas are analyzed in [102] and [20], respectively. The main drawback with the forward scattering results in [43, 44] is that they are only useful when the entire region can be used for the antenna design. They are therefore less useful for antennas integrated (or embedded) into devices such as mobile phones and laptops.

## 6 Antenna current optimization

Optimization can be used to handle simultaneous requirements on the performance and size of complex radiating structures. Here, a typical wireless device structure composed of an antenna region and a ground plane, see Fig. 17 is considered. The entire structure occupies the region denoted  $\Omega$  and consists of *e.g.*, screen, battery, electronics, RF circuitry, antenna(s) etc. for a mobile phone. The antenna, which is part of the structure, is restricted to the region occupying the region  $\Omega_A$ . The antenna designer is assumed to be allowed to specify the spatial distribution of metal and dielectrics in the region  $\Omega_A$ . The electromagnetic properties of the remaining region  $\Omega_G = \Omega \setminus \Omega_A$  is assumed to be fixed. The discussion is restricted to electric current densities and use of the stored energy expression (3.9) and (3.10). Magnetic current densities can in many cases lower the bounds on  $Q$  and can be analyzed using the stored energy expressions in [73, 74].

Many antenna design requirements can be formulated as optimization problems. These problems can be further reformulated as optimization problems in terms of antenna current distributions. An example is presented in the following.

**Antenna design:** From the antenna design perspective, the optimization problem is to design an antenna by proper shaping and choosing of the materials in the antenna region for optimal performance. The current and voltage in one or more feed points determine the matching properties of the antenna. The

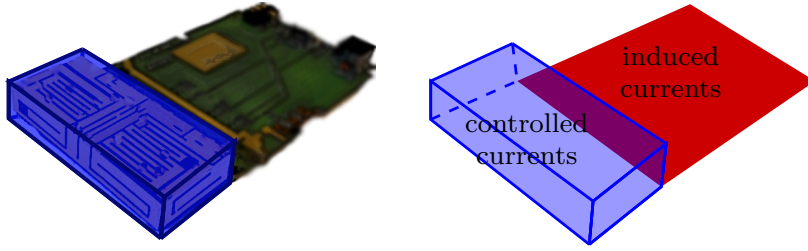


Figure 17: (left) Circumscribing box for an antenna with a ground plane. Physical bounds are determined for arbitrarily shaped antennas inside of a box in the presence of a fixed structure outside of the box. (right) Current optimization with controllable current in the antenna region (the box) and induced current in the remaining structure (here the ground plane).

current distribution in the entire radiating structure determines the radiation properties.

**Current distribution:** In terms of current density, the antenna optimization problem is to determine the currents in the antenna region that yield optimal performance. These currents are determined without considering the feeding structures such that only radiation properties of the antenna are quantified in the performance of the antenna.

## 6.1 Maximization of $G/Q$

The partial gain Q-factor quotient is

$$\frac{G(\hat{\mathbf{r}}, \hat{\mathbf{e}})}{Q} = \frac{4\pi P(\hat{\mathbf{r}}, \hat{\mathbf{e}})}{2\omega \max\{W_e, W_m\}} = \frac{\pi |\hat{\mathbf{e}}^* \cdot \mathbf{F}(\hat{\mathbf{r}})|^2}{\omega \eta_0 \max\{W_e, W_m\}}, \quad (6.1)$$

where  $P(\hat{\mathbf{r}}, \hat{\mathbf{e}})$  is the partial radiation intensity for the polarization  $\hat{\mathbf{e}}$  and direction  $\hat{\mathbf{r}}$ ,  $\mathbf{F}(\hat{\mathbf{r}})$  is the far field (3.7),  $W_e$  is the stored electric energy (3.9), and  $W_m$  is the stored magnetic energy (3.10). The quantities in (6.1) are approximated, using a Method of Moments approach and expanding the current density on the antenna in terms of local basis functions (D.1), as

$$\begin{aligned} \hat{\mathbf{e}}^* \cdot \mathbf{F} &\approx \mathbf{F}\mathbf{I} && \text{far field in direction } \hat{\mathbf{r}} \text{ and polarization } \hat{\mathbf{e}}, \\ W_e &\approx \frac{1}{4\omega} \mathbf{I}^H \mathbf{X}_e \mathbf{I} && \text{stored E-energy, } \mathbf{X}_e \succeq \mathbf{0} \text{ electric reactance,} \\ W_m &\approx \frac{1}{4\omega} \mathbf{I}^H \mathbf{X}_m \mathbf{I} && \text{stored M-energy, } \mathbf{X}_m \succeq \mathbf{0} \text{ magnetic reactance.} \end{aligned}$$

The partial gain Q-factor ratio (6.1) becomes

$$\frac{G(\hat{\mathbf{r}}, \hat{\mathbf{e}})}{Q} \approx \frac{4\pi |\mathbf{F}\mathbf{I}|^2}{\eta_0 \max\{\mathbf{I}^H \mathbf{X}_e \mathbf{I}, \mathbf{I}^H \mathbf{X}_m \mathbf{I}\}}. \quad (6.2)$$



It is assumed that the MoM approximation is sufficiently accurate for the purpose of the analysis.

The optimization problem of maximizing the  $G/Q$  ratio (6.2) can be formulated as the problem of minimizing the stored energy for a fixed partial radiation intensity

$$\begin{aligned} & \text{minimize} && \max\{\mathbf{I}^H \mathbf{X}_e \mathbf{I}, \mathbf{I}^H \mathbf{X}_m \mathbf{I}\} \\ & \text{subject to} && |\mathbf{F}\mathbf{I}|^2 = 1, \end{aligned} \quad (6.3)$$

where the normalization  $|\mathbf{F}\mathbf{I}|^2 = 1$  or equivalently  $|\mathbf{F}\mathbf{I}| = 1$  is used. Formulation (6.3) is possible due to the scaling invariance of  $G/Q$  in terms of the current matrix  $\mathbf{I}$ , *i.e.*,  $G/Q$  is invariant for the complex scaling  $\mathbf{I} \rightarrow \alpha\mathbf{I}$ . Moreover, this scaling invariance shows that an arbitrary phase  $\mathbf{F}\mathbf{I} = 1$  that removes the absolute value operation, [40] can be considered. The convex optimization problem of minimizing the stored energy for a fixed partial far-field in one direction [40], *i.e.*,

$$\begin{aligned} & \text{minimize} && \max\{\mathbf{I}^H \mathbf{X}_e \mathbf{I}, \mathbf{I}^H \mathbf{X}_m \mathbf{I}\} \\ & \text{subject to} && \mathbf{F}\mathbf{I} = 1 \end{aligned} \quad (6.4)$$

is obtained. Let  $\mathbf{I}_o$  denote a current matrix that solves (6.4). The minimum value of the stored energy in (6.4) is unique although the current matrix  $\mathbf{I}_o$  is not necessarily unique. This optimum current gives an upper bound on  $G/Q$  for the considered direction  $\hat{\mathbf{r}}$  and polarization  $\hat{\mathbf{e}}$ , *i.e.*,

$$\frac{G(\hat{\mathbf{r}}, \hat{\mathbf{e}})}{Q} \leq \left. \frac{G(\hat{\mathbf{r}}, \hat{\mathbf{e}})}{Q} \right|_{\text{ub}} = \frac{4\pi |\mathbf{F}\mathbf{I}_o|^2}{\eta_0 \max\{\mathbf{I}_o^H \mathbf{X}_e \mathbf{I}_o, \mathbf{I}_o^H \mathbf{X}_m \mathbf{I}_o\}}. \quad (6.5)$$

Alternative formulations are available for the convex optimization problem (6.4) [40]. These formulations can be solved with *e.g.*, CVX [30], a dual formulation [54], etc., see [36, 40] for illustrations.

The optimization problem (6.4) can be solved analytically in the limit of small antennas [47], giving:

$$\frac{G(\hat{\mathbf{r}}, \hat{\mathbf{e}})}{Q} \leq \frac{k^3}{4\pi} \hat{\mathbf{e}}^* \cdot \boldsymbol{\gamma}_\infty \cdot \hat{\mathbf{e}} \quad \text{and} \quad Q \geq \frac{6\pi}{k^3 \max \text{eig} \boldsymbol{\gamma}_e} \quad \text{as } ka \rightarrow 0 \quad (6.6)$$

for the case of electric,  $W_e \geq W_m$ , antennas. This result confirms the forward scattering bounds (5.4) and (5.5), as also illustrated in Fig. 14. The general case with electric and magnetic current densities is analyzed in [73, 117] and show that electric polarizability dyadic in (6.6) is replaced with the sum of the electric and magnetic polarizability dyadics. The lower bound on the Q-factor for electric dipoles is *e.g.*, [73, 117]

$$Q \geq \frac{6\pi}{k^3 \max \text{eig}(\boldsymbol{\gamma}_e + \boldsymbol{\gamma}_m)} \quad \text{as } ka \rightarrow 0, \quad (6.7)$$

see [73, 117] for additional cases and examples.

## 6.2 Superdirectivity and prescribed radiation patterns

Antennas with a higher directivity than typical antennas of the same size are often referred to as superdirective antennas [8, 56, 79, 84]. The increase of the Q-factor for small antennas with high directivity is analyzed by adding the constraint  $D \geq D_0$  to (6.4). Written in the far-field, the partial directivity is at least  $D_0$  if

$$D_0 \leq D = \frac{4\pi|\hat{\mathbf{e}}^* \cdot \mathbf{F}(\hat{\mathbf{r}})|^2}{2\eta_0 P_r} \Rightarrow P_r \leq \frac{2\pi|\hat{\mathbf{e}}^* \cdot \mathbf{F}(\hat{\mathbf{r}})|^2}{\eta_0 D_0}. \quad (6.8)$$

This is added as the convex constraint  $\frac{1}{2}\mathbf{I}^H \mathbf{R} \mathbf{I} \leq 2\pi/(\eta_0 D_0)$  to the optimization problem (6.4), giving

$$\begin{aligned} & \text{minimize} && \max\{\mathbf{I}^H \mathbf{X}_e \mathbf{I}, \mathbf{I}^H \mathbf{X}_m \mathbf{I}\} \\ & \text{subject to} && \mathbf{F} \mathbf{I} = 1 \\ & && \mathbf{I}^H \mathbf{R} \mathbf{I} \leq \frac{4\pi}{\eta_0 D_0}. \end{aligned} \quad (6.9)$$

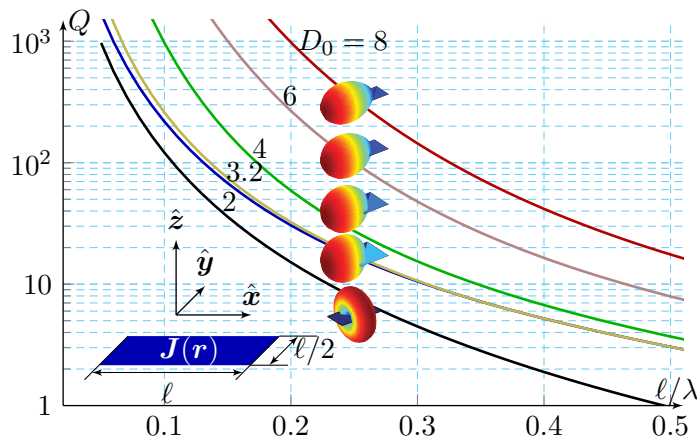


Figure 18: Illustration of the physical bound on the Q-factor for antennas constrained to a planar rectangle with length  $\ell$  and width  $\ell/2$  that radiates with directivity  $D(\hat{\mathbf{x}}) \geq D_0$  for  $D_0 = \{2, 3.2, 4, 6, 8\}$ , see [40].

This optimization problem is solved using CVX [30] for a planar rectangle with side lengths  $\ell$  and  $\ell/2$ , and  $D_0 = \{2, 3.2, 4, 6, 8\}$ . The minimum Q-factor, for a radiated field with the partial directivity at least  $D_0$  in the  $\hat{\mathbf{r}} = \hat{\mathbf{x}}$ -direction for the polarization  $\hat{\mathbf{e}} = \hat{\mathbf{y}}$ , is depicted in Fig. 18. These Q-factors are compared to the Q-factor (5.5) obtained from the forward scattering bound on  $D/Q$  (5.4) for the same rectangle. In the forward scattering bound, it is assumed that the antennas radiate as electric dipoles. Under this assumption, the directivity is 1.5 in a direction normal to the plane of the structure, see Fig. 18, and the generalized absorption efficiency is  $\eta = 1/2$  [43, 45]. Note that the constraints  $D \geq D_0 = \{4, 6, 8\}$  yield optimum current densities with directivities  $D = D_0$ . However, the constraint  $D \geq 2$  results

in an optimum current that contributes both an electric and a magnetic dipole such that the directivity is  $D \geq 2.9$ , for  $\ell/\lambda \geq 0.05$ , see the curves labeled 2 and 3.2 in Fig. 18.

### 6.3 Embedded antennas

The current optimization method can be generalized to derive bounds for antennas embedded in devices, *e.g.*, as that depicted in Fig. 17. This generalization is based on decomposing the current density into the controllable currents,  $\mathbf{J}_A$ , and induced currents,  $\mathbf{J}_G$ , [15, 16, 40]. A region of the considered device,  $\Omega_A$ , see Fig. 21, is reserved for a structure that can be engineered by, *e.g.*, optimization, manual or computer aided design, etc. The currents in this region,  $\mathbf{J}_A$ , are considered controllable. The remaining part of the device,  $\Omega_G$  is considered fixed such that it supports the induced current density  $\mathbf{J}_G$ . Due to the linearity of Maxwell's equations  $\mathbf{J}_G$  depends linearly on  $\mathbf{J}_A$ . This dependence can be written  $\mathbf{J}_G = \mathbf{C}\mathbf{J}_A$ , where  $\mathbf{C}$  is determined from, *e.g.*, the MoM impedance matrix [63, 69, 70, 89]. The bounds on  $G/Q$  of a rectangular, infinitely thin, PEC device with the dimensions  $\ell$  and  $\ell/2$  in which the region with controllable currents may occupy 6%, 10% and 25% of the device at one end in the  $\ell$  direction are depicted in Fig. 19. These bounds are compared to the bound of the entire structure obtained from the forward scattering sum rule described in Sec. 5, see also [43, 44, 45]. Other cases of embedded devices and details can be found in [15, 16, 17, 54].

## 7 Periodic array antennas

Sum rules are used to derive limitations on the bandwidth for array antennas in [22, 75]. The bandwidth of infinite periodic array antennas is limited by the thickness of the array. Consider a periodic array antenna with thickness  $d$  above a perfect electric conducting (PEC) ground plane, see Fig. 20. The antenna performance is analyzed in receiving mode by assuming a reciprocal loss-less antenna with scattering reflection coefficient,  $\rho$ , of equal amplitude as the reflection coefficient in the feed (3.1), *i.e.*,  $|\Gamma| = |\rho|$ . Here, the fundamental mode of the reflected wave is considered. This transforms the antenna to an absorber and the sum rule [22, 75, 94]

$$\frac{1}{\pi} \int_{\mathbb{R}} \frac{1}{k^2} \ln \frac{1}{|\rho(k)|} dk \leq d \left(1 + \frac{\gamma}{2dA}\right) \leq d \max\{\mu_r\} \begin{cases} \cos \theta & \text{TE} \\ 1/\cos \theta & \text{TM} \end{cases} \quad (7.1)$$

first derived by Rozanov [94] for layered structures with  $\max\{\mu_r\}$  denoting the maximal relative permeability of the structure. Here, the low-frequency expansion from [49] is used to extend the results to periodic structures.

The sum rule is transformed to the bandwidth bound [22, 75, 94]

$$\lambda_2 - \lambda_1 \leq \frac{2\pi^2 d \max\{\mu_r\}}{\ln |\Gamma_0|^{-1}} \begin{cases} \cos \theta & \text{TE} \\ 1/\cos \theta & \text{TM} \end{cases} \quad (7.2)$$

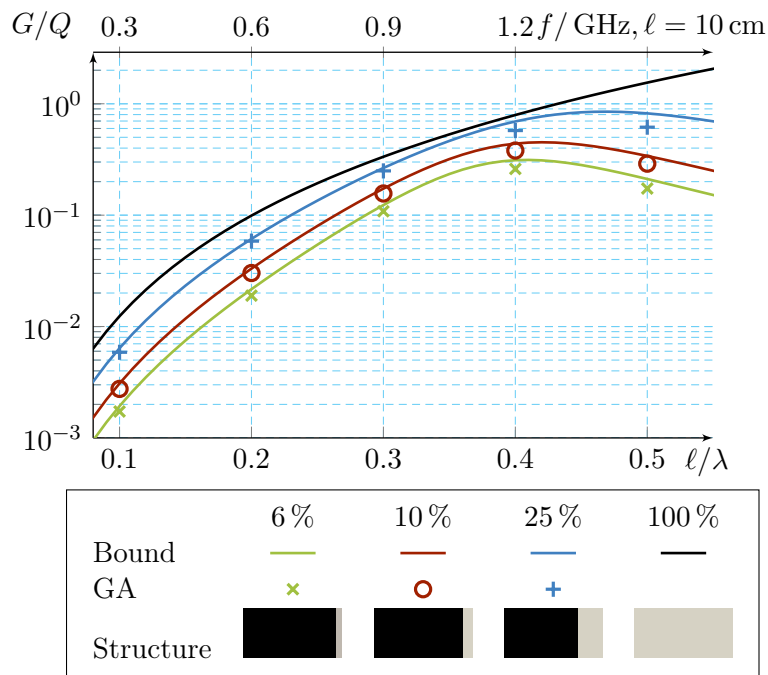


Figure 19: GA-optimized antenna  $G/Q$ -ratios (6.2), marks, compared with physical bounds on  $G/Q$  obtained with a formulation equivalent to (6.4) for a rectangular wireless device model in which the antenna may occupy 6%, 10% and 25% of the device at one end, see Fig. 17. The physical bound on the  $G/Q$ -ratio of a rectangular, infinitely-thin, PEC sheet [43, 44, 45] is labeled “100%”. Gray-shaded areas have controllable currents.

for linearly polarized waves, where  $\Gamma_0$  denotes the threshold level for the reflection coefficient over the wavelength interval  $[\lambda_1, \lambda_2]$ . Array antennas are analyzed and compared with antenna designs in [22, 75]. An array figure of merit is also introduced in [75].

## 8 Conclusions

Physical bounds on antennas answer questions such as: *how good can an antenna be?* The antenna bounds have evolved from spherical regions (1948), to arbitrary shaped structures (2007), and embedded structures (2013). Here, an overview of methods based on circuit models, mode expansions, sum rules, and optimization are presented and some of their pros and cons are discussed. This characterization is chosen to emphasize the key characteristics of the majority of the published methods for the study of physical bounds.

All presented bounds are based on assumptions. The forward-scattering bounds are *e.g.*, based in the assumption of linear, reciprocal, time-translational invariant material parameters. These assumptions are valid for most antennas but switches and non-Foster matching can potentially be used to overcome the limitations [121].

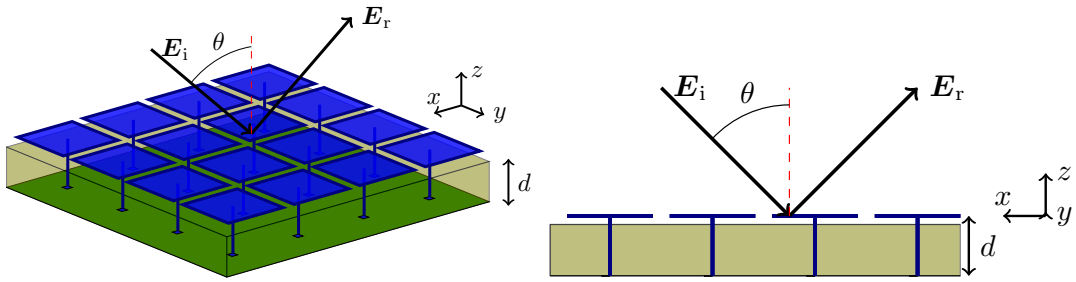


Figure 20: Periodic array antenna above a PEC ground plane.

Moreover, bounds based on the stored energy, such as the Chu bound (4.2) and the antenna current optimization in Sec. 6, assume that the stored energy can be determined accurately using (3.8), (3.9), and (3.10). There are initial investigations on the stored energy expressions [37, 38, 51, 65] but much work remains before the stored energy is fully understood.

Although there have been a strong development on the physical bounds in recent years, there are still many open questions. The  $D/Q$  and Q-factor limits for small electric dipole antennas composed of non-magnetic materials are well understood. There are several independent derivations that provide similar results [35, 40, 43, 44, 47, 114, 117, 118], see also (5.4) and (6.6) for this case. In addition, many antenna designs are shown to perform close to the bounds, see [6, 9, 35, 43, 96] and Fig. 15. Antennas embedded in finite PEC structures are investigated in [15, 16] and are also shown to perform close to the bounds. The  $D/Q$  results for electric dipole antennas work well up to about half-a-wavelength sized structures ( $ka \approx 1.5$ ) [35, 43]. The corresponding lower bounds on the Q-factor for larger structures are not well understood, except for the case with prescribed radiation patterns, *e.g.*, dipole patterns [14, 40, 110].

The case with mixed electric and magnetic dipole patterns, magnetic materials, and superdirective antennas (6.9) are not as well understood in the sense of realized antenna designs although there are some suggested designs. Efficiency is the most important small antenna parameter besides bandwidth. There are only some initial investigations for lossy structures [46], so much work remains on fundamental limitations for efficiency.

## Acknowledgment

This work was supported by the Swedish Research Council (VR) and the Swedish Foundation for Strategic Research (SSF) under the program Applied Mathematics and the project Complex analysis and convex optimization for EM design.

## Appendix A Notation

Scalars are denoted with an italic font ( $f, F$ ), vectors (in  $\mathbb{R}^3$ ) with a boldface italic font ( $\mathbf{f}, \mathbf{F}$ ), and matrices with a boldface roman font ( $\mathbf{f}, \mathbf{F}$ ). We consider time harmonic fields in free space with the time convention  $e^{j\omega t}$ .

---

$c_0$	Speed of light, $c_0 = 1/\sqrt{\epsilon_0\mu_0}$
$\eta_0$	impedance of free space, $\eta_0 = \sqrt{\mu_0/\epsilon_0}$
$\mu_0$	permeability of free space, $\mu_0 = \eta_0/c_0$
$\epsilon_0$	permittivity of free space, $\epsilon_0 = 1/(\eta_0c_0)$
$\epsilon_r$	relative permittivity
$\mu_r$	relative permeability
$\mathbf{E}$	electric field
$\mathbf{H}$	magnetic field
$\mathbf{J}$	current density
$\rho$	charge density, $\rho = \frac{-1}{j\omega} \nabla \cdot \mathbf{J}$
$\mathbf{F}$	far field
$Z_{\text{in}}$	input impedance
$R_{\text{in}}$	input resistance, $R_{\text{in}} = \text{Re } Z_{\text{in}}$
$X_{\text{in}}$	input reactance, $X_{\text{in}} = \text{Im } Z_{\text{in}}$
$W_e$	stored electric energy
$W_m$	stored magnetic energy
$P_d$	dissipated power
$P_r$	radiated power
$P_\Omega$	ohmic losses
$Q$	Q-factor (3.3)
$Q_{Z'}$	Q from $Z'_{\text{in}}$ (3.6)
$\Gamma$	reflection coefficient, see Fig. 6
$\Gamma_0$	threshold level for the reflection coefficient, see Fig. 6
$D$	directivity, also partial directivity $D(\hat{\mathbf{r}}, \hat{\mathbf{e}})$
$G$	gain, also partial gain $G(\hat{\mathbf{r}}, \hat{\mathbf{e}})$
$\gamma_e$	electric polarizability dyadic
$\gamma_m$	magnetic polarizability dyadic
$\gamma_\infty$	high contrast polarizability dyadic (C.1)
$\mathbf{r}$	position vector in $\mathbb{R}^3$ , see Fig. 7
$r$	magnitude of $\mathbf{r}$ , <i>i.e.</i> , $r =  \mathbf{r} $ , see Fig. 7
$r_{12}$	distance $ \mathbf{r}_1 - \mathbf{r}_2 $
$\hat{\mathbf{r}}$	(unit) direction vector, <i>i.e.</i> , $\hat{\mathbf{r}} = \mathbf{r}/r$ , see Fig. 7
$\hat{\mathbf{e}}$	(unit) polarization vector, see Fig. 7
$\Omega$	source region, see Fig. 7
$\Omega_A$	antenna region, $\Omega_A \subset \Omega$ , see Fig. 17
$\Omega_G$	ground plane region, see Fig. 17
$a$	radius of a circumscribing sphere, see Fig. 8
$\ell$	side length of a rectangle, also $\ell_x, \ell_y$
$f$	frequency

$\omega$	angular frequency $\omega = 2\pi f$
$k$	wavenumber $k = \omega/c$
$\lambda$	wavelength $\lambda = c/f$
$B$	fractional bandwidth (3.2)
$\psi$	basis function (D.1)
$\mathbf{I}$	current matrix
$\mathbf{Z}$	impedance matrix (D.2)
$\mathbf{R}$	resistance matrix, $\mathbf{R} = \text{Re } \mathbf{Z}$
$\mathbf{X}$	reactance matrix, $\mathbf{X} = \text{Im } \mathbf{Z}$
$\mathbf{X}_e$	electric reactance matrix (D.5)
$\mathbf{X}_m$	magnetic reactance matrix (D.5)
$\mathbf{F}$	far-field matrix
$\mathbf{C}$	induced currents matrix
$j$	imaginary unit, $j^2 = -1$
$*$	complex conjugate, $(a + jb)^* = a - jb$
$\text{T}$	transpose
$\text{H}$	Hermitian transpose
$\succeq$	positive semidefinite, $\mathbf{I}^{\text{H}} \mathbf{A} \mathbf{I} \geq 0$ for all $\mathbf{I}$
$\hat{\cdot}$	unit vector, $ \hat{\mathbf{r}}  = 1$
$\nabla$	nabla operator
$dV$	volume element
$dS$	surface element

---

## Appendix B Radial functions

The radial functions in Hansen [55] are defined as

$$\mathbf{R}_{\tau n}^{(p)}(\kappa) = \begin{cases} z_n^{(p)}(\kappa) & \tau = 1 \\ \frac{1}{\kappa} \frac{\partial(\kappa z_n^{(p)}(\kappa))}{\partial \kappa}, & \tau = 2, \end{cases} \quad (\text{B.1})$$

where  $z_n^{(1)} = j_n$  are Bessel functions,  $z_n^{(2)} = n_n$  Neumann functions,  $z_n^{(3)} = h_n^{(1)}$  Hankel functions [55], and  $\kappa = ka$ . The derivatives of  $\mathbf{R}_{\tau n}^{(p)}(\kappa)$  are easily expressed in spherical Bessel and Hankel functions as

$$\frac{\partial \mathbf{R}_{\tau n}^{(p)}}{\partial \kappa} = \begin{cases} \frac{\partial}{\partial \kappa} z_n^{(p)} & \tau = 1 \\ \frac{-\mathbf{R}_{\tau n}^{(p)}}{\kappa} + \frac{n(n+n) - \kappa^2}{\kappa^2} z_n^{(p)} & \tau = 2. \end{cases} \quad (\text{B.2})$$

## Appendix C High-contrast polarizability dyadics

The high-contrast polarizability dyadics have closed form expressions for canonical geometries such as spheres and spheroids, see [82], Tab. 2, and the MATLAB program [45]. Other shapes are analyzed numerically using integral equation solvers such as the method of moments.



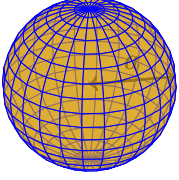
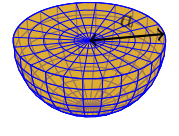
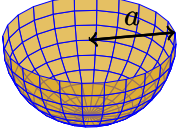
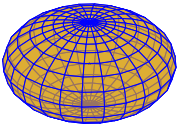
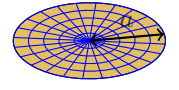
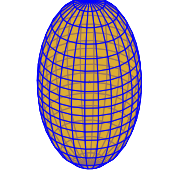
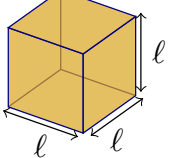
geometry	high contrast polarizability dyadic $\gamma_\infty$
	Sphere with radius $a$ [82] $\gamma_\infty = \gamma_{\text{sph}} \mathbf{1} = 4\pi a^3 \mathbf{1} \approx 12.57a^3 \mathbf{1}$
	Solid hemisphere with radius $a$ [82] $\gamma_\infty = 4\pi \left(2 - \frac{59}{27\sqrt{3}}\right) a^3 (\hat{x}\hat{x} + \hat{y}\hat{y}) + \frac{4}{27\sqrt{3}} \left(\frac{64}{3} - \frac{25}{16}(\sqrt{3} + 1)\right) a^3 \hat{z}\hat{z}$ $\approx 9.28a^3 (\hat{x}\hat{x} + \hat{y}\hat{y}) + 4.59a^3 \hat{z}\hat{z} \approx 0.74\gamma_{\text{sph}} (\hat{x}\hat{x} + \hat{y}\hat{y}) + 0.36\gamma_{\text{sph}} \hat{z}\hat{z}$
	Hemispherical shell with radius $a$ [82] $\gamma_\infty = \left(2\pi + \frac{8}{3}\right) a^3 (\hat{x}\hat{x} + \hat{y}\hat{y}) + \left(2\pi - \frac{16}{3} + \frac{4\pi}{2 + \pi}\right) a^3 \hat{z}\hat{z}$ $\approx 8.95a^3 (\hat{x}\hat{x} + \hat{y}\hat{y}) + 3.39a^3 \hat{z}\hat{z} \approx 0.71\gamma_{\text{sph}} (\hat{x}\hat{x} + \hat{y}\hat{y}) + 0.27\gamma_{\text{sph}} \hat{z}\hat{z}$
	Oblate spheroid with width $2a$ and height $2b$ , where $b \leq a$ [82, 103]. Set $\xi = b/a$ and $e = \sqrt{1 - \xi^2}$ $\gamma_\infty = \frac{4\pi\xi e^3}{3(e - \xi \arccos \xi)} a^3 (\hat{x}\hat{x} + \hat{y}\hat{y}) + \frac{8\pi e^3}{3(\arccos \xi - \xi e)} a^3 \hat{z}\hat{z}$
	Circular disc with radius $a$ [44] $\gamma_\infty = \frac{16}{3} a^3 (\hat{x}\hat{x} + \hat{y}\hat{y}) \approx 5.33a^3 (\hat{x}\hat{x} + \hat{y}\hat{y}) \approx 0.42\gamma_{\text{sph}} (\hat{x}\hat{x} + \hat{y}\hat{y})$
	Prolate spheroid with height $2a$ and width $2b$ , where $b \leq a$ [82, 103]. Set $\xi = b/a$ and $e = \sqrt{1 - \xi^2}$ $\gamma_\infty = \frac{8\pi e^3}{3(\ln \frac{1+e}{1-e} - 2e)} a^3 (\hat{x}\hat{x} + \hat{y}\hat{y}) + \frac{16\pi\xi^2 e^3}{3(2e - \xi^2 \ln \frac{1+e}{1-e})} a^3 \hat{z}\hat{z}$ $\approx \frac{4\pi}{3(\ln 2 - \ln \xi - 1)} a^3 \hat{z}\hat{z} + O(\xi^2) \quad \text{as } \xi \rightarrow 0$
	Cube with side lengths $\ell = 2a/\sqrt{3}$ [66, 98] $\gamma_\infty \approx 3.644305190268\ell^3 \mathbf{1} \approx 5.61a^3 \mathbf{1} \approx 0.45\gamma_{\text{sph}} \mathbf{1}$

Table 2: High-contrast polarizability dyadics for some canonical structures. The body-of-revolution objects have  $\hat{z}$  as the symmetry axis, see also Fig. 14 and [45].

The high-contrast polarizability dyadic  $\boldsymbol{\gamma}_\infty$  is determined from the induced surface charge density,  $\rho$ , as

$$\hat{\mathbf{e}} \cdot \boldsymbol{\gamma}_\infty \cdot \hat{\mathbf{e}} = \frac{1}{E_0 \epsilon_0} \int_{\partial\Omega} \hat{\mathbf{e}} \cdot \mathbf{r} \rho(\mathbf{r}) \, dS, \quad (\text{C.1})$$

where  $\rho$  satisfies the integral equation

$$\int_{\partial\Omega} \frac{\rho(\mathbf{r}_1)}{4\pi\epsilon_0|\mathbf{r} - \mathbf{r}_1|} \, dS_1 = E_0 \mathbf{r} \cdot \hat{\mathbf{e}} - V \quad (\text{C.2})$$

and the voltage  $V$  determined is from the constraints of zero total charge

$$\int_{\partial\Omega} \rho(\mathbf{r}) \, dS = 0. \quad (\text{C.3})$$

## Appendix D Expansion in terms of basis functions

Consider a region  $\Omega \subset \mathbb{R}^3$  with current density  $\mathbf{J} = \mathbf{J}(\mathbf{r})$ , see Fig. 7. Expand the current density in local basis functions

$$\mathbf{J}(\mathbf{r}) \approx \sum_{n=1}^N I_n \boldsymbol{\psi}_n(\mathbf{r}) \quad (\text{D.1})$$

and introduce the  $N \times 1$  matrix  $\mathbf{I}$  with elements  $I_n$  to simplify the notation. The basis functions are assumed to be real valued, divergence conforming, and having vanishing normal components at the boundary [89]. For embedded antennas, it is assumed that the currents  $\mathbf{J}_A$  in the antenna region  $\Omega_A$  are controllable and induce the currents  $\mathbf{J}_G$  in the region  $\Omega_G$ , see Fig. 21.

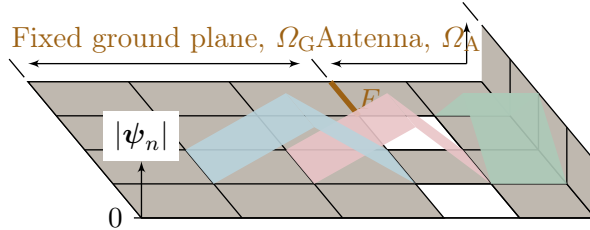


Figure 21: Illustration of rectangular mesh element discretization and “rooftop” basis function amplitude for a three-dimensional radiating structure. Metal areas are depicted in gray shading. The amplitudes of three of the total  $6 \times 3 + 5 \times 4 - 4 - 3$  basis functions are depicted in blue, pink and green shading. The feeding edge is marked  $F$ .

A standard MoM implementation of the EFIE using the Galerkin procedure computes the impedance matrix  $\mathbf{Z} = \mathbf{R} + j\mathbf{X}$  with the elements

$$\frac{Z_{mn}}{\eta_0} = j \int_{\partial\Omega} \int_{\partial\Omega} (k^2 \boldsymbol{\psi}_m(\mathbf{r}_1) \cdot \boldsymbol{\psi}_n(\mathbf{r}_2) - \nabla_1 \cdot \boldsymbol{\psi}_m(\mathbf{r}_1) \nabla_2 \cdot \boldsymbol{\psi}_n(\mathbf{r}_2)) \frac{e^{-jk|\mathbf{r}_1 - \mathbf{r}_2|}}{4\pi k |\mathbf{r}_1 - \mathbf{r}_2|} \, dS_1 \, dS_2, \quad (\text{D.2})$$

where  $m, n = 1, \dots, N$ . The differentiated MoM impedance matrix

$$\begin{aligned} \frac{k}{\eta_0} \frac{\partial Z_{mn}}{\partial k} = & \int_{\partial\Omega} \int_{\partial\Omega} \mathbf{j} \left( k^2 \boldsymbol{\psi}_m(\mathbf{r}_1) \cdot \boldsymbol{\psi}_n(\mathbf{r}_2) + \nabla_1 \cdot \boldsymbol{\psi}_m(\mathbf{r}_1) \nabla_2 \cdot \boldsymbol{\psi}_n(\mathbf{r}_2) \right) \frac{e^{-jk|\mathbf{r}_1 - \mathbf{r}_2|}}{4\pi k |\mathbf{r}_1 - \mathbf{r}_2|} \\ & + \left( k^2 \boldsymbol{\psi}_m(\mathbf{r}_1) \cdot \boldsymbol{\psi}_n(\mathbf{r}_2) - \nabla_1 \cdot \boldsymbol{\psi}_m(\mathbf{r}_1) \nabla_2 \cdot \boldsymbol{\psi}_n(\mathbf{r}_2) \right) \frac{e^{-jk|\mathbf{r}_1 - \mathbf{r}_2|}}{4\pi} dS_1 dS_2 \quad (\text{D.3}) \end{aligned}$$

is used to estimate the stored energy determined. The differentiated reactance matrix,  $\mathbf{X}' = \text{Im} \mathbf{Z}'$ , gives the stored magnetic and electric energies

$$W_m \approx \frac{1}{8} \mathbf{I}^H \left( \frac{\partial \mathbf{X}}{\partial \omega} + \frac{\mathbf{X}}{\omega} \right) \mathbf{I} \quad \text{and} \quad W_e \approx \frac{1}{8} \mathbf{I}^H \left( \frac{\partial \mathbf{X}}{\partial \omega} - \frac{\mathbf{X}}{\omega} \right) \mathbf{I}, \quad (\text{D.4})$$

respectively. These expressions are identical to the stored energy expressions introduced by Vandebosch [113] using a MoM approximations, see also [62, 64]. Introduce the electric  $\mathbf{X}_e$ , and magnetic  $\mathbf{X}_m$ , reactance matrices

$$\mathbf{X}_e = \frac{1}{2} \left( \omega \frac{\partial \mathbf{X}}{\partial \omega} - \mathbf{X} \right) \quad \text{and} \quad \mathbf{X}_m = \frac{1}{2} \left( \omega \frac{\partial \mathbf{X}}{\partial \omega} + \mathbf{X} \right). \quad (\text{D.5})$$

The total radiated power is determined from  $\mathbf{R} = \text{Re}\{\mathbf{Z}\}$  as

$$P_{\text{rad}} \approx \frac{1}{2} \mathbf{I}^H \mathbf{R} \mathbf{I}. \quad (\text{D.6})$$

The far field (3.7) in the direction  $\hat{\mathbf{r}}$  projected on  $\hat{\mathbf{e}}$  is approximated by the  $N \times 1$  matrix  $\mathbf{F} \mathbf{I} \approx \hat{\mathbf{e}}^* \cdot \mathbf{F}(\hat{\mathbf{r}})$  defined as

$$\mathbf{F} \mathbf{I} \approx -jk\eta_0 \sum_{n=1}^N I_n \int_{\partial\Omega} \hat{\mathbf{e}}^* \cdot \boldsymbol{\psi}_n(\mathbf{r}_1) \frac{e^{jk\hat{\mathbf{r}} \cdot \mathbf{r}_1}}{4\pi} dS_1. \quad (\text{D.7})$$

In this paper it is assumed that the numerical approximation is sufficiently accurate so the approximate equal to ( $\approx$ ) above can be replaced with equalities.

## Appendix E Numerical results for the presented antennas

Numerical simulation data for the antennas presented in this chapter are collected in Tab. 3 for wire antennas and Tab. 4 for planar antennas.

## Appendix References

- [1] J. J. Adams et al. ‘‘Conformal printing of electrically small antennas on three-dimensional surfaces’’. *Advanced Materials* 23.11 (2011), pp. 1335–1340.
- [2] S. A. Altair Development S.A. (Pty) Ltd Stellenbosch. *FEKO, Field Computations Involving Bodies of Arbitrary Shape, Suite 7.0*. 2014.








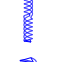

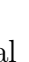
	$\ell_1/\ell_2$	$ka$	$D$	$Q$	$\frac{D}{Q(ka)^3}$	$\frac{4\pi D}{Q\gamma k^3}$
	100	1.481	1.63	5	0.094	1.00
	50	1.463	1.63	5	0.116	1.00
	20	1.188	1.61	7	0.139	0.82
	10	1.184	1.61	7	0.145	0.59
	1	0.587	1.50	19	0.388	0.69
	0.01	1.075	2.34	5	0.369	0.83
	2	0.421	1.50	49	0.411	0.86
	1	0.137	1.50	675	0.867	0.87
	3	0.497	1.49	29	0.425	0.85
	1.5	0.266	1.50	142	0.557	0.83

Table 3: Numerical results of the wire antennas simulated in FEKO [2], see also Fig. 15. The forward scattering bounding boxes are either cylindrical or spheroidal depending on the geometry of the structure.

- [3] A. Bernland. “Bandwidth limitations for scattering of higher order electromagnetic spherical waves with implications for the antenna scattering matrix”. *IEEE Trans. Antennas Propagat.* 60.9 (2012), pp. 4345–4353.
- [4] A. Bernland, M. Gustafsson, and S. Nordebo. “Physical limitations on the scattering of electromagnetic vector spherical waves”. *J. Phys. A: Math. Theor.* 44.14 (2011), p. 145401.
- [5] A. Bernland, A. Luger, and M. Gustafsson. “Sum rules and constraints on passive systems”. *J. Phys. A: Math. Theor.* 44.14 (2011), p. 145205.
- [6] S. R. Best. “Electrically small resonant planar antennas: optimizing the quality factor and bandwidth.” *IEEE Antennas and Propagation Magazine* 57.3 (2015), pp. 38–47.
- [7] S. R. Best. “The radiation properties of electrically small folded spherical helix antennas”. *IEEE Trans. Antennas Propagat.* 52.4 (2004), pp. 953–960.
- [8] S. R. Best et al. “An impedance-matched 2-element superdirective array”. *Antennas and Wireless Propagation Letters, IEEE* 7 (2008), pp. 302–305.
- [9] S. R. Best. “A comparison of the cylindrical folded helix Q to the Gustafsson limit”. In: *Antennas and Propagation, 2009. EuCAP 2009. 3rd European Conference on.* IEEE. 2009, pp. 2554–2557.




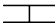





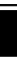
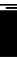
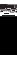
	$\ell_1/\ell_2$	$ka$	$D$	$Q$	$\frac{D}{Q(ka)^3}$	$\frac{4\pi D}{Q\gamma k^3}$
	100	1.486	1.64	6	0.078	0.99
	10	1.319	1.62	7	0.105	0.64
	5	1.178	1.61	7	0.132	0.61
	0.33	1.072	1.47	37	0.032	0.61
	10	1.411	1.64	4	0.157	0.96
	0.67	1.246	2.48	12	0.109	0.70
	5	0.953	1.59	12	0.148	0.68
	5	1.050	1.57	7	0.194	0.89
	2	0.708	1.55	18	0.245	0.86
	2	1.359	1.67	3	0.260	0.91
	2	0.953	1.53	19	0.095	0.33
	2	0.351	1.51	257	0.136	0.47

Table 4: Numerical results of the planar antennas simulated in FEKO [2], see also Fig. 15. Results are for a rectangular forward scattering bounding box.

- [10] S. R. Best and D. L. Hanna. “A performance comparison of fundamental small-antenna designs”. *Antennas and Propagation Magazine, IEEE* 52.1 (2010), pp. 47–70.
- [11] J. G. van Bladel. *Electromagnetic Fields*. Second Edition. IEEE Press, 2007.
- [12] C. J. Carpenter. “Electromagnetic energy and power in terms of charges and potentials instead of fields”. *IEE Proc. A* 136.2 (1989), pp. 55–65.
- [13] D. K. Cheng. *Field and wave electromagnetics*. Addison-Wesley, 1989.
- [14] L. J. Chu. “Physical limitations of omnidirectional antennas”. *J. Appl. Phys.* 19 (1948), pp. 1163–1175.
- [15] M. Cismasu and M. Gustafsson. “Antenna bandwidth optimization with single frequency simulation”. *IEEE Trans. Antennas Propagat.* 62.3 (2014), pp. 1304–1311.
- [16] M. Cismasu and M. Gustafsson. “Multiband antenna Q optimization using stored energy expressions”. *IEEE Antennas and Wireless Propagation Letters* 13.2014 (2014), pp. 646–649.

- [17] M. Cismasu, D. Tayli, and M. Gustafsson. *Stored Energy Based 3D Antenna Analysis and Design*. Tech. rep. LUTEDX/(TEAT-7231)/1-18/(2014). Lund University, 2014.
- [18] R. E. Collin and S. Rothschild. “Evaluation of antenna Q”. *IEEE Trans. Antennas Propagat.* 12 (1964), pp. 23–27.
- [19] W. Davis et al. “Fundamental limits on antenna size: a new limit”. *Microwaves, Antennas Propagation, IET* 5.11 (2011), pp. 1297–1302.
- [20] A. Derneryd et al. “Application of gain-bandwidth bounds on loaded dipoles”. *IET Microwaves, Antennas & Propagation* 3.6 (2009), pp. 959–966.
- [21] J. P. Doane, K. Sertel, and J. L. Volakis. “Bandwidth limits for lossless, reciprocal PEC-backed arrays of arbitrary polarization”. *IEEE Trans. Antennas Propagat.* 62.5 (2014), pp. 2531–2542.
- [22] J. P. Doane, K. Sertel, and J. L. Volakis. “Matching bandwidth limits for arrays backed by a conducting ground plane”. *IEEE Trans. Antennas Propagat.* 61.5 (2013), pp. 2511–2518.
- [23] R. M. Fano. “Theoretical limitations on the broadband matching of arbitrary impedances”. *Journal of the Franklin Institute* 249.1,2 (1950), 57–83 and 139–154.
- [24] R. L. Fante. “Quality factor of general antennas”. *IEEE Trans. Antennas Propagat.* 17.2 (1969), pp. 151–155.
- [25] H. D. Foltz and J. S. McLean. “Limits on the radiation Q of electrically small antennas restricted to oblong bounding regions”. In: *IEEE Antennas and Propagation Society International Symposium*. Vol. 4. IEEE. 1999, pp. 2702–2705.
- [26] W. Geyi. “A method for the evaluation of small antenna Q”. *IEEE Trans. Antennas Propagat.* 51.8 (2003), pp. 2124–2129.
- [27] W. Geyi. “Physical limitations of antenna”. *IEEE Trans. Antennas Propagat.* 51.8 (2003), pp. 2116–2123.
- [28] W. Geyi. *Foundations of Applied Electrodynamics*. John Wiley & Sons, 2011.
- [29] A. A. Glazunov, M. Gustafsson, and A. Molisch. “On the physical limitations of the interaction of a spherical aperture and a random field”. *IEEE Trans. Antennas Propagat.* 59.1 (2011), pp. 119–128.
- [30] M. Grant and S. Boyd. *CVX: Matlab Software for Disciplined Convex Programming, version 1.21*. <http://cvxr.com/cvx>. 2011.
- [31] D. J. Griffiths. *Introduction to Electrodynamics*. Third. Prentice-Hall, Inc., 1999.
- [32] M. Gustafsson. “Physical bounds on antennas of arbitrary shape”. In: *Antennas and Propagation Conference (LAPC), 2011 Loughborough*. IEEE. 2011, pp. 1–5.

- [33] M. Gustafsson. “Sum rules for lossless antennas”. *IET Microwaves, Antennas & Propagation* 4.4 (2010), pp. 501–511.
- [34] M. Gustafsson. “Time-domain approach to the forward scattering sum rule”. *Proc. R. Soc. A* 466 (2010), pp. 3579–3592.
- [35] M. Gustafsson, M. Cismasu, and S. Nordebo. “Absorption efficiency and physical bounds on antennas”. *International Journal of Antennas and Propagation* 2010.Article ID 946746 (2010), pp. 1–7.
- [36] M. Gustafsson, J. Friden, and D. Colombi. “Antenna current optimization for lossy media with near field constraints”. *Antennas and Wireless Propagation Letters, IEEE* 14 (2015), pp. 1538–1541.
- [37] M. Gustafsson and B. L. G. Jonsson. “Antenna Q and stored energy expressed in the fields, currents, and input impedance”. *IEEE Trans. Antennas Propagat.* 63.1 (2015), pp. 240–249.
- [38] M. Gustafsson and B. L. G. Jonsson. “Stored electromagnetic energy and antenna Q”. *Progress In Electromagnetics Research (PIER)* 150 (2015), pp. 13–27.
- [39] M. Gustafsson and S. Nordebo. “On the spectral efficiency of a sphere”. *Progress in Electromagnetics Research* 67 (2007), pp. 275–296.
- [40] M. Gustafsson and S. Nordebo. “Optimal antenna currents for Q, superdirectivity, and radiation patterns using convex optimization”. *IEEE Trans. Antennas Propagat.* 61.3 (2013), pp. 1109–1118.
- [41] M. Gustafsson and D. Sjöberg. “Sum rules and physical bounds on passive metamaterials”. *New Journal of Physics* 12 (2010), p. 043046.
- [42] M. Gustafsson and C. Sohl. “New physical bounds on elliptically polarized antennas”. In: *Proceedings of the Third European Conference on Antennas and Propagation*. The Institution of Engineering and Technology. 2009, pp. 400–402.
- [43] M. Gustafsson, C. Sohl, and G. Kristensson. “Illustrations of new physical bounds on linearly polarized antennas”. *IEEE Trans. Antennas Propagat.* 57.5 (2009), pp. 1319–1327.
- [44] M. Gustafsson, C. Sohl, and G. Kristensson. “Physical limitations on antennas of arbitrary shape”. *Proc. R. Soc. A* 463 (2007), pp. 2589–2607.
- [45] M. Gustafsson. *AntennaQ—MATLAB script that computes physical bounds on Q and D/Q for antennas*.  
<http://www.mathworks.se/matlabcentral/fileexchange/26806-antennaq>. 2010.
- [46] M. Gustafsson. “Efficiency and Q for small antennas using Pareto optimality”. In: *Antennas and Propagation Society International Symposium (APSURSI)*. IEEE. 2013, pp. 2203–2204.



- [47] M. Gustafsson, M. Cismasu, and B. L. G. Jonsson. “Physical bounds and optimal currents on antennas”. *IEEE Trans. Antennas Propagat.* 60.6 (2012), pp. 2672–2681.
- [48] M. Gustafsson and S. Nordebo. “Bandwidth, Q factor, and resonance models of antennas”. *Progress in Electromagnetics Research* 62 (2006), pp. 1–20.
- [49] M. Gustafsson and D. Sjöberg. “Physical bounds and sum rules for high-impedance surfaces”. *IEEE Trans. Antennas Propagat.* 59.6 (2011), pp. 2196–2204.
- [51] M. Gustafsson, D. Tayli, and M. Cismasu. *Q factors for antennas in dispersive media*. Tech. rep. LUTEDX/(TEAT-7232)/1–24/(2014). Lund University, 2014.
- [52] M. Gustafsson et al. “Optical theorem and forward scattering sum rule for periodic structures”. *IEEE Trans. Antennas Propagat.* 60.8 (2012), pp. 3818–3826.
- [53] M. Gustafsson et al. “Physical bounds and sum rules in scattering and antenna theory”. In: *International Conference on Electromagnetics in Advanced Applications (ICEAA)*. 2009, pp. 600–603.
- [54] M. Gustafsson et al. “Tutorial on antenna current optimization using MATLAB and CVX”. 2016.
- [55] J. E. Hansen, ed. *Spherical Near-Field Antenna Measurements*. IEE electromagnetic waves series 26. Peter Peregrinus Ltd., 1988.
- [56] R. C. Hansen. *Electrically Small, Superdirective, and Superconductive Antennas*. John Wiley & Sons, 2006.
- [57] R. C. Hansen. “Fundamental limitations in antennas”. *Proc. IEEE* 69.2 (1981), pp. 170–182.
- [58] R. C. Hansen and R. E. Collin. “A new Chu formula for Q”. *IEEE Antennas and Propagation Magazine* 51.5 (2009), pp. 38–41.
- [59] R. C. Hansen and R. E. Collin. *Small Antenna Handbook*. Wiley, 2011.
- [60] T. V. Hansen, O. S. Kim, and O. Breinbjerg. “Stored energy and quality factor of spherical wave functions—in relation to spherical antennas with material cores”. *IEEE Trans. Antennas Propagat.* 60.3 (2012), pp. 1281–1290.
- [61] R. F. Harrington. *Time Harmonic Electromagnetic Fields*. McGraw-Hill, 1961.
- [62] R. Harrington. “Characteristic modes for antennas and scatterers”. English. In: *Numerical and Asymptotic Techniques in Electromagnetics*. Ed. by R. Mittra. Vol. 3. Topics in Applied Physics. Springer Berlin Heidelberg, 1975, pp. 51–87.
- [63] R. F. Harrington. *Field Computation by Moment Methods*. Macmillan, 1968.
- [64] R. F. Harrington and J. R. Mautz. “Control of radar scattering by reactive loading”. *IEEE Trans. Antennas Propagat.* 20.4 (1972), pp. 446–454.



- [65] P. Hazdra, M. Capek, and J. Eichler. “Radiation Q-factors of thin-wire dipole arrangements”. *Antennas and Wireless Propagation Letters, IEEE* 10 (2011), pp. 556–560.
- [66] J. Helsing and K.-M. Perfekt. “On the polarizability and capacitance of the cube”. *Applied and Computational Harmonic Analysis* 34.3 (2013), pp. 445–468.
- [67] IEEE145-1993. *IEEE Standard Definition of Terms for Antennas*. Antenna Standards Committee of the IEEE Antennas and Propagation Society. 1993.
- [68] J. D. Jackson. *Classical Electrodynamics*. Third. John Wiley & Sons, 1999.
- [69] J. M. Jin. *Theory and Computation of Electromagnetic Fields*. Wiley, 2011.
- [70] J. M. Johnson and Y. Rahmat-Samii. “Genetic algorithms and method of moments GA/MOM for the design of integrated antennas”. *IEEE Trans. Antennas Propagat.* 47.10 (1999), pp. 1606–1614.
- [71] D. S. Jones. “Scattering by inhomogeneous dielectric particles”. *Quart. J. Mech. Appl. Math.* 38 (1985), pp. 135–155.
- [72] R. C. Jones. “A generalization of the dielectric ellipsoid problem”. *Phys. Rev.* 68.3–4 (1945), pp. 93–96.
- [73] B. L. G. Jonsson and M. Gustafsson. “Stored energies in electric and magnetic current densities for small antennas”. *Proc. R. Soc. A* 471.2176 (2015), p. 20140897.
- [74] B. L. G. Jonsson and M. Gustafsson. “Stored energies for electric and magnetic currents with applications to Q for small antennas”. In: *Electromagnetic Theory (EMTS), Proceedings of 2013 URSI International Symposium on*. IEEE. 2013, pp. 1050–1053.
- [75] B. L. G. Jonsson, C. I. Kolitsidas, and N Hussain. “Array antenna limitations”. *Antennas and Wireless Propagation Letters, IEEE* 12 (2013), pp. 1539–1542.
- [76] D. Kajfez Jr and W. P. Wheless. “Invariant definitions of the unloaded Q factor”. *IEEE Trans. Microwave Theory Tech.* 34.7 (1986), pp. 840–841.
- [77] A. Karlsson. “Physical limitations of antennas in a lossy medium”. *IEEE Trans. Antennas Propagat.* 52 (2004), pp. 2027–2033.
- [78] P.-S. Kildal and S. R. Best. “Further investigations of fundamental directivity limitations of small antennas with and without ground planes”. In: *Antennas and Propagation Society International Symposium, 2008. AP-S 2008. IEEE*. IEEE. 2008, pp. 1–4.
- [79] O. Kim, S. Pivnenko, and O. Breinbjerg. “Superdirective magnetic dipole array as a first-order probe for spherical near-field antenna measurements”. *IEEE Trans. Antennas Propagat.* 60.10 (2012), pp. 4670–4676.
- [80] O. Kim. “Minimum Q electrically small antennas”. *IEEE Trans. Antennas Propagat.* 60.8 (2012), pp. 3551–3558.

- [81] O. Kim, O. Breinbjerg, and A. Yaghjian. “Electrically small magnetic dipole antennas with quality factors approaching the chu lower bound”. *IEEE Trans. Antennas Propagat.* 58.6 (2010), pp. 1898–1906.
- [82] R. E. Kleinman and T. B. A. Senior. “Rayleigh scattering”. In: *Low and high frequency asymptotics*. Ed. by V. V. Varadan and V. K. Varadan. Vol. 2. Handbook on Acoustic, Electromagnetic and Elastic Wave Scattering. Elsevier Science Publishers, 1986. Chap. 1, pp. 1–70.
- [83] D.-H. Kwon. “On the radiation Q and the gain of crossed electric and magnetic dipole moments”. *IEEE Trans. Antennas Propagat.* 53.5 (2005), pp. 1681–1687.
- [84] D. Margetis et al. “Highly directive current distributions: general theory”. *Physical Review E* 58.2 (1998), p. 2531.
- [85] J. S. McLean. “A re-examination of the fundamental limits on the radiation Q of electrically small antennas”. *IEEE Trans. Antennas Propagat.* 44.5 (1996), pp. 672–676.
- [86] S. Nordebo, M. Gustafsson, and G. Kristensson. “On the capacity of the free space antenna channel”. In: *IEEE Antennas and Propagation Society International Symposium 2006*, IEEE Press. 2006, pp. 3105–3108.
- [87] H. M. Nussenzveig. *Causality and dispersion relations*. Academic Press, 1972.
- [88] D. Nyberg, P.-S. Kildal, and J. Carlsson. “Effects of intrinsic radiation Q on mismatch factor of three types of small antennas: single-resonance, gradual-transition and cascaded-resonance types”. English. *IET Microwaves, Antennas & Propagation* 4 (1 2010), 83–90(7).
- [89] A. F. Peterson, S. L. Ray, and R. Mittra. *Computational Methods for Electromagnetics*. IEEE Press, 1998.
- [90] D. M. Pozar. *Microwave Engineering*. John Wiley & Sons, 1998.
- [91] D. M. Pozar. “New results for minimum Q, maximum gain, and polarization properties of electrically small arbitrary antennas”. In: *Antennas and Propagation, 2009. EuCAP 2009. 3rd European Conference on*. 2009, pp. 1993–1996.
- [92] E. M. Purcell. “On the absorption and emission of light by interstellar grains”. *J. Astrophys.* 158 (1969), pp. 433–440.
- [93] J. Rahola. “Bandwidth potential and electromagnetic isolation: Tools for analysing the impedance behaviour of antenna systems”. In: *Antennas and Propagation, 2009. EuCAP 2009. 3rd European Conference on*. 2009, pp. 944–948.
- [94] K. N. Rozanov. “Ultimate thickness to bandwidth ratio of radar absorbers”. *IEEE Trans. Antennas Propagat.* 48.8 (2000), pp. 1230–1234.
- [95] M. Shahpari, D. Thiel, and A. Lewis. “An investigation into the Gustafsson limit for small planar antennas using optimization”. *IEEE Trans. Antennas Propagat.* 62.2 (2014), pp. 950–955.

- [96] M. Shahpari, D. V. Thiel, and A. Lewis. “Polarizability of 2D and 3D conducting objects using method of moments”. *ANZIAM Journal* 54 (2013), pp. C446–C458.
- [97] D. F. Sievenpiper et al. “Experimental validation of performance limits and design guidelines for small antennas”. *IEEE Trans. Antennas Propagat.* 60.1 (2012), pp. 8–19.
- [98] A. Sihvola et al. “Polarizabilities of platonic solids”. *IEEE Trans. Antennas Propagat.* 52.9 (2004), pp. 2226–2233.
- [99] D. Sjöberg. “Variational principles for the static electric and magnetic polarizabilities of anisotropic media with perfect electric conductor inclusions”. *J. Phys. A: Math. Theor.* 42 (2009), p. 335403.
- [100] A. K. Skrivervik et al. “PCS antenna design: the challenge of miniaturization”. *IEEE Antennas and Propagation Magazine* 43.4 (2001), pp. 12–27.
- [101] A. K. Skrivervik and M. Gustafsson. “Fundamental limitations”. In: *Handbook on small antennas*. Ed. by L. Joffre et al. EurAAP seventh framework programme. Universitat Politecnica de Catalunya, 2012, pp. 5–59.
- [102] C. Sohl and M. Gustafsson. “A priori estimates on the partial realized gain of Ultra-Wideband (UWB) antennas”. *Quart. J. Mech. Appl. Math.* 61.3 (2008), pp. 415–430.
- [103] C. Sohl, M. Gustafsson, and G. Kristensson. “Physical limitations on broadband scattering by heterogeneous obstacles”. *J. Phys. A: Math. Theor.* 40 (2007), pp. 11165–11182.
- [104] C. Sohl et al. “A scattering and absorption identity for metamaterials: experimental results and comparison with theory”. *J. Appl. Phys.* 103.5 (2008), p. 054906.
- [105] J. C.-E. Sten, P. K. Koivisto, and A. Hujanen. “Limitations for the radiation  $Q$  of a small antenna enclosed in a spheroidal volume: axial polarisation”. *AEÜ Int. J. Electron. Commun.* 55.3 (2001), pp. 198–204.
- [106] H. Stuart, S. Best, and A. Yaghjian. “Limitations in relating quality factor to bandwidth in a double resonance small antenna”. *Antennas and Wireless Propagation Letters* 6 (2007).
- [107] T. T. Taylor. “Design of line-source antennas for narrow beamwidth and low side lobes”. *Antennas and Propagation, Transactions of the IRE Professional Group on* 3.1 (1955), pp. 16–28.
- [108] H. L. Thal. “Exact circuit analysis of spherical waves”. *IEEE Trans. Antennas Propagat.* 26.2 (1978), pp. 282–287.
- [109] H. L. Thal. “Gain and  $Q$  bounds for coupled TM-TE modes”. *IEEE Trans. Antennas Propagat.* 57.7 (2009), pp. 1879–1885.
- [110] H. L. Thal. “New radiation  $Q$  limits for spherical wire antennas”. *IEEE Trans. Antennas Propagat.* 54.10 (2006), pp. 2757–2763.

- [111] H. L. Thal. “Q Bounds for Arbitrary Small Antennas: A Circuit Approach”. *IEEE Trans. Antennas Propagat.* 60.7 (2012), pp. 3120–3128.
- [112] G. Thiele, P. Detweiler, and R. Penno. “On the lower bound of the radiation Q for electrically small antennas”. *IEEE Trans. Antennas Propagat.* 51.6 (2003), pp. 1263–1269.
- [113] G. A. E. Vandenbosch. “Reactive energies, impedance, and Q factor of radiating structures”. *IEEE Trans. Antennas Propagat.* 58.4 (2010), pp. 1112–1127.
- [114] G. A. E. Vandenbosch. “Simple procedure to derive lower bounds for radiation Q of electrically small devices of arbitrary topology”. *IEEE Trans. Antennas Propagat.* 59.6 (2011), pp. 2217–2225.
- [115] J. Volakis, C. C. Chen, and K. Fujimoto. *Small Antennas: Miniaturization Techniques & Applications*. McGraw-Hill, 2010.
- [116] H. A. Wheeler. “Fundamental limitations of small antennas”. *Proc. IRE* 35.12 (1947), pp. 1479–1484.
- [117] A. D. Yaghjian, M. Gustafsson, and B. L. G. Jonsson. “Minimum Q for lossy and lossless electrically small dipole antennas”. *Progress In Electromagnetics Research* 143 (2013), pp. 641–673.
- [118] A. D. Yaghjian and H. R. Stuart. “Lower bounds on the Q of electrically small dipole antennas”. *IEEE Trans. Antennas Propagat.* 58.10 (2010), pp. 3114–3121.
- [119] A. D. Yaghjian and S. R. Best. “Impedance, bandwidth, and Q of antennas”. *IEEE Trans. Antennas Propagat.* 53.4 (2005), pp. 1298–1324.
- [120] A. H. Zemanian. *Distribution theory and transform analysis: an introduction to generalized functions, with applications*. Dover Publications, 1987.
- [121] R. W. Ziolkowski, M.-C. Tang, and N. Zhu. “An efficient, broad bandwidth, high directivity, electrically small antenna”. *Microwave and Optical Technology Letters* 55.6 (2013), pp. 1430–1434.